High-density transposon mutagenesis in *Mycobacterium abscessus* identifies an essential penicillin-binding lipo-protein (PBP-lipo) involved in septal peptidoglycan synthesis and antibiotic sensitivity

Chidiebere Akusobi[1], Bouchra S. Benghomari[2], Junhao Zhu[1], Ian D. Wolf[1], Shreya Singhvi[3], Charles L. Dulberger[1], Thomas R. Ioerger[4], Eric J. Rubin[1]

[1]Department of Immunology and Infectious Diseases, Harvard T.H. Chan School of Public Health, Boston, MA 02115, USA

[2]Department of Biology, Northeastern University, Boston, MA 02115, USA

[3]Department of Molecular and Cell Biology, University of California, Berkeley, Berkeley, CA 94720, USA

[4]Department of Computer Science and Engineering, Texas A&M University, College Station Texas 77843, USA

Abstract

Mycobacterium abscessus (*Mab*) is a rapidly growing non-tuberculous mycobacterium (NTM) that causes a wide range of infections. Treatment of *Mab* infections is difficult because the bacterium is intrinsically resistant to many classes of antibiotics. Developing new and effective treatments against *Mab* requires a better understanding of the unique vulnerabilities that can be targeted for future drug development. To achieve this, we identified essential genes in *Mab* by conducting transposon-sequencing (TnSeq) on the reference *Mab* strain ATCC 19977. We generated ~51,000 unique transposon mutants and used this high-density library to identify 362 essential genes for *in vitro* growth. To investigate species-specific vulnerabilities in *Mab*, we further characterized *MAB_3167c*, a predicted penicillin-binding-lipoprotein (PBP-lipo) that is essential in *Mab* and non-essential in *Mycobacterium tuberculosis* (*Mtb*). We found that PBP-lipo primarily localizes to the subpolar region and later to the septum as cells prepare to divide. Depletion of *Mab* PBP-lipo causes cells to elongate, develop ectopic branches, and form multiple septa. Knockdown of PBP-lipo along with PbpB, DacB1, and a carboxypeptidase, MAB_0519 lead to synergistic growth arrest. In contrast, these genetic interactions were absent in the *Mtb* model organism, *Mycobacterium smegmatis*, indicating that the PBP-lipo homologs in the two species exist in distinct genetic networks. Finally, repressing PBP-lipo sensitized the reference strain and 11 *Mab* clinical isolates to several classes of antibiotics, including the β-lactams, ampicillin and amoxicillin by greater than 128-fold. Altogether, this study presents PBP-lipo as a key enzyme to study *Mab* specific processes in cell wall synthesis and importantly positions PBP-lipo as an attractive drug target to treat *Mab* infections.

Introduction

Mycobacterium abscessus (*Mab*) is the most common cause of human disease among the rapidly growing non-tuberculous mycobacteria (NTM). It causes a wide range of illnesses including lung, skin and soft-tissue infections, as well as disseminated disease (1–3). While the incidence of *Mab* infections is rising worldwide, treating *Mab* infections remains difficult. The bacterium has intrinsic and acquired resistance mechanisms to many classes of antibiotics, including the standard drugs used to treat tuberculosis (4,5). The current treatment regimen for *Mab* requires taking a combination of multiple antibiotics for up to 18 months and is often associated with severe toxicity and routinely ends in treatment failure (6). Thus, there is an urgent need for new and effective drugs to treat the emerging global public health threat of *Mab* infections (7).

Developing novel antibiotic treatments for *Mab* requires a better understanding of essential biological processes in the bacterium that can be targeted. Identifying essential genes is the first step in this process, and by combining transposon-mutagenesis with massive parallel sequencing, transposon-sequencing (TnSeq) has been an effective tool to determine gene essentiality on a genome-wide scale in other microbes (8). However, while many TnSeq screens have been conducted in *Mycobacterium tuberculosis* (*Mtb*) (9), up until recently, only two *Mab* TnSeq screens have been published (10,11). While both *Mab* TnSeq screens provided tools and important insights into *Mab* biology, neither utilized a mutant library with high enough density to comprehensively identify essential genes. This changed with the recent publication from Rifat *et al*, who generated robust high-density transposon libraries of *Mab* and identified a comprehensive list of genetic elements essential for *in vitro* growth (12). Identification of these essential genes serves as an excellent starting point to classify attractive targets for drug discovery.

66 One major target of antibiotics is the mycobacterial cell wall whose biogenesis is essential for
67 bacterial growth (13,14). The structure of the mycobacterial cell wall is unique among bacteria
68 because it is composed of three macromolecules: peptidoglycan (PG), arabinogalactan, and
69 mycolic acids. Together, these layers envelop mycobacteria with a thick, waxy coat that forms a
70 permeability barrier to many drugs (15,16). The foundational layer is comprised of peptidoglycan
71 (PG), which consists of glycan sugars cross-linked by short peptides forming a continuous, net-
72 like structure that maintains cell shape and prevents rupture. Mycobacteria build new PG at the
73 cell poles aided by Class A penicillin binding proteins (PBPs) that perform two reactions: a
74 transglycosylation reaction that polymerizes PG monomers to existing glycan strands and a
75 transpeptidation reaction that cross-links glycan strands to each other (17). Class B PBPs solely
76 perform the cross-linking reactions (18,19). A hallmark of PBPs is that they are inhibited by β-
77 lactam antibiotics; however, these antibiotics are typically not used to treat *Mab* infections due
78 to high levels of resistance and the presence of β-lactamases in the genome (20).
79
80 To identify essential genes for *in vitro* growth and classify potential new drug targets in *Mab*, we
81 performed TnSeq. We generated high-density transposon libraries of ~51,000 mutants in the
82 reference strain, *M. abscessus subsp. abscessus* ATCC 19977 and identified 362 genes
83 required for *in vitro* growth. We next identified essential genes in *Mab* that were non-essential in
84 *Mtb* in order to study species-specific vulnerabilities in *Mab*. From this list of genes, we further
85 characterized *MAB_3167c*, which encodes PBP-lipo, a conserved Class B PBP. We found that
86 PBP-lipo is required for normal peptidoglycan (PG) synthesis and cell division. Knockdown of
87 PBP-lipo sensitizes *Mab* to commonly-used β-lactams and other classes of antibiotics. None of
88 these phenotypes were present in the *Mycobacterium smegmatis (Msm)* and *Mtb* PBP-lipo
89 knockouts. Thus, we find that PBP-lipo has a unique essential function in *Mab* and is a potential
90 drug target for treating *Mab* infections.

Results

Identification of *M. abscessus* ATCC 19977 essential genes for *in vitro* growth

To identify essential genes in *Mab*, we performed TnSeq on *M. abscessus subsp. abscessus* ATCC 19977 (hereafter referred to as *Mab*) using the ϕMycoMar T7 phage carrying the Himar1 transposon for transduction. This transposon inserts into 'TA' dinucleotide sites and disrupts gene function (Figure 1A) (21). We transduced three independently grown cultures of *Mab*, yielding triplicate libraries with saturations of 54.2%, 62.3%, and 64.1% for Library 1, 2, and 3 respectively (Supplemental Table 1). The average Pearson r^2 correlation of mean read counts for each gene across 2 libraries was 0.85 indicating good correlation among the libraries (Supplemental Figure 1). The transposon insertions across the three libraries were mapped onto the *Mab* genome (Figure 1B). Across three libraries, we generated approximately 51,000 unique transposon mutants, as defined by sites of unique transposon insertions across all three libraries. Of note, the *Mab* libraries shared the same non-permissive 'TA' sites for transposon insertion as has been described in other mycobacterial species (22).

The high density of these libraries allowed us to identify essential *Mab* genes using the Hidden Markov Model (HMM) algorithm implemented in TRANSIT (23). HMM identified 362 genes as essential, 4167 as non-essential, 153 as producing a growth defect when disrupted, and 233 as causing a growth advantage when disrupted (Figure 1C, Supplemental Table 2). As expected, many of the genes identified as essential were involved in key biological processes including protein translation, amino acid metabolism, and cell wall biogenesis based on Clusters of Orthologous Groups (COG) analysis (Figure 1E).

Identification and validation of uniquely essential genes in *Mab*

Understanding differences in essential genes between *Mab* and *Mtb* might uncover new ways of specifically targeting *Mab*. Thus, we identified *Mab*-specific essential genes by comparing gene

118 essentiality between mutual orthologs of *Mab* and *Mtb.* We used *Mtb* essentiality data
119 generated from a comprehensive analysis using 14 high-quality TnSeq datasets (9). Of the
120 2279 mutual orthologs between *Mab* and *Mtb*, 282 genes were essential in both species. We
121 focused on the mutual orthologs that that were essential in *Mab,* but non-essential in *Mtb*.
122 These genes could potentially represent *Mab* specific drug targets. Exactly 20 genes fit into this
123 category, which we refer to as "uniquely essential" (Figure 1D) (Supplemental Table 3).
124
125 To understand the quality of predictions by TnSeq, we validated the essentiality of a subset of
126 genes using an anhydrotetracycline (ATc) inducible CRISPRi system developed for use in *Mtb*
127 (24). Expression of a non-targeting sgRNA control in this system had no impact on cell
128 proliferation (Figure 2A). In contrast, repressing canonical essential genes *rpoB, gyrB,* and *secY*
129 impaired cell growth in both liquid broth (Figure 2A) and solid media (Supplemental Figure 2A),
130 indicating that the CRISPRi system developed in *Mtb* functions in *Mab*.
131
132 We next validated the essentiality of a subset of the 20 uniquely essential genes in *Mab*: *glnA2,*
133 *icd2, sdhA,* and *MAB_4471*. CRISPRi knockdown of these uniquely essential genes impaired
134 growth in liquid media (Figure 2B) as well as solid media (Supplemental Figure 2B). These
135 results confirm that at least a subset of uniquely essential *Mab* genes identified by TnSeq are
136 required for optimal *in vitro* growth. The slight rise in OD_{600} later in the time course is consistent
137 with the emergence of escape mutants in the CRISPRi system, which has been previously
138 described (25,26).
139
140 **PBP-lipo is uniquely essential in *Mab***
141 One of the uniquely essential genes we identified was *MAB_3167c*, which encodes a
142 hypothesized Class B penicillin-binding lipoprotein (PBP-lipo). PBP-lipo is predicted to have a
143 single N-terminal transmembrane helix and a transpeptidase domain. We found that

144 *MAB_3167c* lacked transposon insertions across all three replicate libraries (Figure 3A). This
145 finding corroborates data from previously generated *Mab* transposon libraries that show lack of
146 insertions in *MAB_3167c* (10,12). Comparing the essentiality of PBP enzymes in *Mab* with their
147 homologs in *Mtb* revealed that *MAB_3167c* is unique in being the sole PBP whose essentiality
148 differs between the two species. Specifically, PBP-lipo is essential in *Mab* and non-essential in
149 *Mtb* (Figure 3B).
150
151 To validate that PBP-lipo is required for *in vitro* growth, we used the CRISPRi system to induce
152 knockdown using constructs encoding 1, 2, or 3 sgRNAs targeting *MAB_3167c* (Supplemental
153 Figure 3A). The single, double, and triple sgRNA constructs allowed for the fine tuning of the
154 magnitude of PBP-lipo knockdown, as measured by RT-qPCR (Supplemental Figure 3B). We
155 noted that the empty vector control (0 sgRNA) and single sgRNA construct had no detectable
156 effect on the growth of *Mab* (Supplemental Figure 3C). In contrast, when *MAB_3167c* was
157 targeted with either 2 or 3 sgRNAs, the growth of *Mab* was inhibited, indicating that PBP-lipo is
158 indeed required for optimal *in vitro* growth (Figure 3C). We also observed inhibition of cell
159 growth on solid media where knockdown of PBP-lipo by 2 sgRNA and 3 sgRNA vectors led to a
160 1000-fold reduction in colony forming units (CFU) (Supplemental Figure 3D). In contrast to *Mab*,
161 when we deleted the gene encoding PBP-lipo in *Mtb*, *Rv2864c*, the growth of the knockout and
162 wild-type strains was indistinguishable (Figure 3D). Similarly, the PBP-lipo homolog in *Msm,*
163 *MSMEG_2584c*, when knocked out grew identically to wildtype with no growth defect
164 (Supplemental Figure 4).
165
166 To complement the PBP-lipo knockdown growth defect phenotype in *Mab*, we recoded a
167 version of PBP-lipo with the protospacer adjacent motif (PAM) and sgRNA binding sequences
168 mutated while preserving the amino acid sequence. This prevents sgRNAs from binding the
169 exogenous PBP-lipo copy present on the integrated plasmid. When constitutively expressed,

170 this recoded PBP-lipo rescued growth of the native PBP-lipo knockdown (Figure 3E). In
171 contrast, a recoded allele that was predicted to be catalytically inactive (S364A) did not rescue
172 growth. All together, this data demonstrates that PBP-lipo's predicted transpeptidase activity is
173 required for *Mab* optimal growth, while PBP-lipo's activity in *Mtb* and *Msm* is non-essential.
174
175 **PBP-lipo is required to maintain normal cell elongation and division**
176 A hallmark of PBPs is that they bind β-lactam antibiotics. Therefore, to test whether PBP-lipo is
177 an active PBP in *Mab*, we determined whether PBP-lipo binds bocillin FL, a fluorescent analog
178 of penicillin (27). Using a strain that constitutively expresses a strep-tagged PBP-lipo, we
179 identified a fluorescent bocillin FL band at the same molecular weight as PBP-lipo, which was
180 confirmed to be PBP-lipo by Western blot (Supplemental Figure 5A). These data suggest that
181 PBP-lipo binds bocillin FL *in vivo* and is an active PBP. Interestingly, in wildtype *Mab,* we did not
182 detect an obvious PBP-lipo band at the predicted molecular weight of PBP-lipo, 63 kDa,
183 suggesting that native expression levels of PBP-lipo is either low or PBP-lipo is expressed at
184 distinct periods during the cell cycle.
185
186 We also tested whether PBP-lipo was indeed a lipoprotein. Based on its amino acid sequence,
187 PBP-lipo has a N-terminal signal sequence that targets the protein for localization to the
188 periplasm. This is followed by a conserved cysteine residue, which is the canonical site of lipid
189 modification (28). To determine if PBP-lipo is lipidated, we performed a lipoprotein extraction
190 protocol to isolate lipoproteins in *Mab* (29). By Western Blot, we successfully detected the
191 presence of PBP-lipo in the lipoprotein fraction (Supplemental Figure 5B). PBP-lipo being
192 present also in the non-lipoprotein fraction is not surprising as similar results were observed in
193 early lipoprotein extraction experiments performed in *Mtb* (30)
194

195 In mycobacteria, the PG layer is critical for maintaining normal cell shape and altering PBP
196 expression often results in abnormal cell morphology. Thus, we studied the morphology of *Mab*
197 when PBP-lipo was repressed and discovered dramatic morphological changes. *Mab* cells
198 elongate, branch inappropriately, and form ectopic poles of active growth, as evidenced by
199 staining with NADA (3-[(7-Nitro-2,1,3-benzoxadiazol-4-yl)amino]-D-alanine), a fluorescent-D-
200 amino acid (FDAA) that binds areas of active PG synthesis (31) (Figure 4A). PBP-lipo
201 knockdown significantly increased the number of cells with ectopic branches (Supplemental
202 Figure 6B). Furthermore, during normal growth of *Mab*, a small percentage of cells contain one
203 mid-cell FDAA band, indicating active PG synthesis at the site of septation. However, when
204 PBP-lipo is knocked down, we occasionally find cells with 2 or 3 bands mid-cell, as exemplified
205 in the 2 sgRNA + panel (Figure 4A). PBP-lipo knockdown strains were all significantly longer
206 than their uninduced controls, with the longest average cell length belonging to the strain with
207 the strongest PBP-lipo knockdown (Figure 4B). Of note, while the 0 sgRNA +/- cells are
208 morphologically indistinguishable, there is a statistically significant difference in the mean cell
209 lengths, likely due to the effect of ATc on cells (Figure 4B). Interestingly, cell width did not
210 change among the strains (Supplemental Figure 6A). In comparison, in *Msm* and *Mtb*, there
211 were no significant differences in morphology and cell length between the wildtype and PBP-lipo
212 knockout strains (Supplemental Figure 7). The dramatic changes in *Mab* morphology when
213 PBP-lipo is repressed suggests proper expression levels of this enzyme is required for
214 maintaining normal elongation and division in *Mab.*
215
216 **PBP-lipo localizes to the septum after FtsZ**
217 The morphological defects caused by PBP-lipo knockdown were reminiscent of septal factor
218 depletions observed in *Msm* (32). Thus, we hypothesized that PBP-lipo localizes to the septum.
219 To test this hypothesis, we N-terminally tagged PBP-lipo with mRFP, which has been previously
220 shown to function in the mycobacterial periplasm (33). We cloned mRFP after the predicted N-

221 terminal signal sequence of PBP-lipo with linkers on the 5' and 3' ends of the fluorescent protein
222 (Supplementary Figure 8A). We next validated that this construct produced a full-length fusion
223 protein using Western Blot, and detected the correctly sized 91kDa fusion product
224 (Supplementary Figure 8B). Finally, we tested the functionality of the mRFP-PBP-lipo fusion
225 protein by using recoded and non-recoded versions of the construct. The recoded version had a
226 single sgRNA binding site on PBP-lipo mutated (Supplementary Figure 8A). As expected,
227 knockdown of native PBP-lipo lead to growth inhibition while expression of the non-recoded
228 fusion protein partially complemented growth. Reassuringly, the recoded mRFP-PBP-lipo fully
229 complemented the growth defect from the native PBP-lipo knockdown indicating that the fusion
230 protein is indeed functional.
231
232 Given the morphological defects in the PBP-lipo knockdown, we hypothesized that PBP-lipo
233 localized to the septum. To test this, we imaged PBP-lipo simultaneously with FtsZ, which forms
234 the Z-ring at the divisome. FtsZ is the first protein to localize to the septum and recruits other
235 members of the divisome complex to aid in the formation of the septum and eventual division of
236 the cell (34). To visualize FtsZ, we C-terminally tagged it with mNeonGreen (mNG) and
237 expressed the fusion protein using a weak promoter as higher levels of expression are toxic.
238 After introducing both constructs into wildtype *Mab*, we visualized the fusion proteins, which
239 were expressed in the presence of wildtype PBP-lipo. Using fluorescence microscopy, we
240 discovered that both FtsZ and PBP-lipo localized to the mid-cell, likely in the growing septum.
241 We also identified cells with septal co-localization of both PBP-lipo and FtsZ (Figure 5A).
242
243 The resulting images were analyzed using the recently published MOMIA and GEMATRIA
244 programs, which quantify the fluorescent signal across cells normalized by cell length (35). We
245 first analyzed cells that expressed solely mRFP-PBP-lipo and demonstrated that mid-cell
246 localization of PBP-lipo was only present in the longest cells in the population (Figure 5B).

247 These data demonstrate that as cells elongate, PBP-lipo localizes to the septum and is
248 therefore likely involved in septum formation and cell division. We next applied this analysis to
249 cells that co-expressed mRFP-PBP-lipo and FtsZ-mNG. We found that FtsZ localizes to the
250 septum earlier in the cell life cycle as demonstrated by the higher septal fluorescence signal
251 intensity in shorter cells (Figure 5C). In contrast, PBP-lipo localizes to the septum when cells are
252 longer and after FtsZ has already localized to the septum (Figure 5C). This sequential
253 recruitment of divisome proteins is well described in several bacteria, including *Msm* (32).
254 Localization of FtsZ determines the location of the septum, followed by recruitment of PBPs
255 involved in septal PG synthesis and finally enzymes that aid in daughter cell separation (17).
256 Our data shows the temporal dynamics of FtsZ and PBP-lipo septal localization as well as
257 highlights cells where septal co-localization of both proteins can be appreciated.
258

259 **Knockdown of PBP-lipo disrupts FtsZ regulation and localization**

260 PBP-lipo repression leads to elongated and branched cells with multiple sites of septation as
261 demonstrated by FDAA staining (Figure 4A). This indicates that PBP-lipo repression disrupts
262 the regulation of cell division in *Mab*. We hypothesized this could be due to dysregulated
263 formation of the FtsZ rings responsible for initiating division. To test this hypothesis, we
264 visualized FtsZ in the context of native PBP-lipo knockdown. We used an N-terminal GFP-FtsZ
265 fusion protein expressed off the FtsZ natural promoter to best capture the natural dynamics of
266 expression. Upon PBP-lipo knockdown, we identified cells that formed multiple FtsZ puncta in
267 contrast to the single puncta found in normally growing cells (Figure 5D). These multiple FtsZ
268 puncta were distributed across the length of the cell indicating that repression of PBP-lipo
269 disrupts FtsZ localization. Furthermore, the formation of multiple FtsZ rings likely leads to the
270 creation of multiple septa and eventually the ectopic branching events observed when PBP-lipo
271 is repressed.
272

273 **PBP-lipo is incorporated into a unique PG network in *Mab* that does not exist in *Msm***

274 Given that *Mtb* and *Msm* do not have duplicates of PBP-lipo in their genomes, we hypothesized
275 that there is a functional difference between PBP-lipo in *Mab* and its homologs in *Msm* and *Mtb*.
276 This possibility intrigued us because an alignment of PBP-lipo from various mycobacteria
277 revealed that PBP-lipo$_{Mab}$ has 5 additional amino acids present only in the *Mab* homolog
278 (Supplemental Figure 9A). When *in silico* structures of PBP-lipo$_{Mab}$ and PBP-lipo$_{Mtb}$ are
279 modeled, these 5 extra residues form an appendage we hypothesized could impart PBP-lipo$_{Mab}$
280 with additional ability to bind proteins (Supplemental Figure 9B).

281

282 To test this hypothesis, we constitutively expressed PBP-lipo$_{Msm}$ in the 2 sgRNA *Mab* strain
283 (hereafter referred to as the *Msm* complement strain). As expected, knockdown of the native
284 *Mab* PBP-lipo impairs growth. However, PBP-lipo$_{Msm}$ expression in the 2 sgRNA strain rescued
285 *Mab* growth (Figure 6A). Furthermore, expressing PBP-lipo$_{Msm}$ eliminated the branching
286 phenotype of the native PBP-lipo knockdown and partially reversed the elongated phenotype as
287 well (Figure 6B). The recoded version of PBP-lipo$_{Mab}$ also reversed the branching of cells and
288 partially complemented the elongated phenotype (Figure 6B). In contrast, the catalytically-
289 inactive version of PBP-lipo$_{Mab}$-(S364A) did not complement, with cells remaining elongated and
290 branched (Figure 6B, Supplemental Figure 10). These results demonstrate that PBP-lipo$_{Msm}$ can
291 rescue knockdown of the endogenous *Mab* enzyme. From these data, we conclude that the
292 essentiality of PBP-lipo$_{Mab}$ is not solely due to a unique functional property that is present only in
293 the *Mab* homolog.

294

295 An alternative hypothesis is PBP-lipo participates in a PBP interaction network in *Mab* that is
296 distinct from respective PBP networks in *Msm* and *Mtb*. In short, while PBP-lipo is required in
297 the *Mab* PBP network, its function is likely redundant in the networks of *Msm* and *Mtb.* This
298 notion of functionally distinct PBP networks has been previously described in mycobacteria (36).

299 To interrogate the PBP network of *Mab*, we tested which PBPs genetically interacted with PBP-
300 lipo. To perform this experiment, we cloned CRISPRi constructs with sgRNAs that would weakly
301 knockdown each PBP in *Mab* (PBPx), so that growth was not significantly impaired. We also
302 cloned combinatorial CRISPRi constructs where PBP-lipo and another PBP were weakly
303 repressed. Using this dual sgRNA vector, we could simultaneously knockdown PBP-lipo and a
304 PBP of interest.
305
306 Using combinatorial knockdowns of each PBP, we compared growth inhibition when a single
307 PBP was knocked down versus when PBP-lipo and a second PBP were jointly repressed. Of
308 the 8 combinations we tested, we found that knockdown of three PBPs with PBP-lipo lead to
309 synergistic growth arrest (Figure 6C). These genes were *pbpB, dacB1,* and *MAB_0519,* which
310 encodes a protein with a hypothesized carboxypeptidase domain. This genetic synergy was
311 also observed in liquid culture for *pbpB* and *dacB1* (Supplemental Figure 11A). The homolog of
312 PbpB is a well-studied enzyme in both *Msm, Mtb,* and the model organisms *E. coli* and *B.*
313 *subtilis,* where it is known as FtsI. In all these organisms, PbpB localizes to the septum and is
314 largely responsible for septal PG synthesis (37–39). Interestingly, overexpression of PbpB
315 rescued the growth defect caused by knockdown of PBP-lipo (Supplemental Figure 11B).
316 Similarly, exogenous expression of PbpB fully reversed the morphological defects of PBP-lipo
317 repression (Supplemental Figure 11C). These data indicate that PBP-lipo and PbpB have
318 overlapping functions at the septum in *Mab*. However, because both enzymes are individually
319 essential, PbpB and PBP-lipo must have distinct functions as well.
320
321 To test the importance of the genetic interaction of DacB1 with PBP-lipo, we created a DacB1-
322 GFP fusion, which we validated as being fully intact by Western Blot (Supplemental Figure
323 12A). Interestingly, like PbpB and PBP-lipo, DacB1 localizes to the septum (Supplemental
324 Figure 12B). We also observed co-localization of DacB1 and PBP-lipo at the septal region of the

325 cell (Supplemental Figure 12C). Using the MOMIA and GEMATRIA programs, we quantified the
326 fluorescent signal from DacB1 and PBP-lipo at the septum and binned the cells by cell length.
327 These analyses demonstrate that both DacB1 and PBP-lipo localize to the septum as cells
328 elongate, with DacB1 arriving slightly before PBP-lipo to the septum (Supplemental Figure 12D).
329 These data suggest that PBP-lipo genetically interacts with PbpB and DacB1, and that all three
330 enzymes localize to the same region of the cell and could potentially coordinate septal PG
331 synthesis in a complex together.
332
333 The difference in essentiality of PBP-lipo in different species could be due to altered genetic
334 interactions. To test this in *Msm,* we used CRISPRi to knockdown *Msm* PBP homologues in the
335 wildtype *Msm* and the PBP-lipo knockout background. In this experiment, genes that interacted
336 with PBP-lipo would show impaired cell growth when repressed in the PBP-lipo knockout.
337 Interestingly, we did not observe genetic interactions between any of the PBPs tested and PBP-
338 lipo (Figure 6D). Importantly, the level of knockdown for genes that showed synergy in *Mab* was
339 comparable to the level of knockdown in the *Msm* PBP-lipo knockout, as measured by qPCR
340 (Supplemental Figure 13A). We also did not detect synergy in additional PBPs present in the
341 *Msm* genome with no known homologs in *Mab* (Supplemental Figure 13B).
342
343 These results might suggest that *Msm* PBP-lipo might have different interacting partners. To
344 test this, we generated high density transposon mutant libraries in both the wildtype and PBP-
345 lipo knockout strains of *Msm* to identify genes that were conditionally essential in the knockout
346 background. The saturation of the 2 wildtype libraries were 51.9% and 53.4%, while the
347 saturation of the PBP-lipo knockout library was 62.4%. Using the resampling method in
348 TRANSIT, our TnSeq data revealed that there were no conditionally essential genes in the
349 ΔPBP-lipo *Msm* background (Supplemental Table 4). These data strongly suggest PBP-lipo in
350 *Msm* exists in a robust genetic network with multiple functional redundancies. To uncover PBP-

351 lipo's function in *Msm*, it is possible that double and triple knockout mutants of PG synthesis
352 enzymes would need to be generated.
353
354 **Repressing PBP-lipo sensitizes *Mab* to a wide range of antibiotics**
355 Given PBP-lipo's essentiality in *Mab* and the genetic interactions it has with other PBPs, we
356 hypothesized that repressing PBP-lipo would affect *Mab*'s sensitivity to antibiotics, including β-
357 lactams. To test this hypothesis, we measured the sensitivity of PBP-lipo knockdown cells to 21
358 antibiotics that target translation, transcription, and DNA replication in both *Mab* and *Msm*.
359
360 Wildtype *Mab* is typically resistant to β-lactams amoxicillin and ampicillin with MICs greater than
361 >256 µg/ml. When PBP-lipo is knocked down, the MIC for both antibiotics dropped to 2 µg/ml,
362 indicating a greater than 128-fold sensitization (Table 1). These results indicate a strong
363 chemical-genetic interaction between PBP-lipo and both ampicillin and amoxicillin. Interestingly,
364 not all β-lactams had shifts in their MIC when PBP-lipo was knocked down. This suggests that
365 there is a specific chemical-genetic interaction between PBP-lipo or its partner PBPs and
366 ampicillin and amoxicillin. MIC changes for other β-lactams were less drastic, with a 4-8- fold
367 reduction observed for faropenem and cefoxitin (Table 1). PBP-lipo knockdown also affects
368 susceptibility to antibiotics that do not target the cell wall. The macrolides, clarithromycin and
369 erythromycin, were 128-fold and 64-fold more potent respectively in the PBP-lipo knock down
370 cells. A 16-fold reduction in MIC was also observed for RNA polymerase inhibitor, rifampicin.
371
372 The MIC differences in rifampicin and clarithromycin are notable because these antibiotics do
373 not target the cell wall. Thus, the mechanism of synergy between PBP-lipo repression and these
374 antibiotics likely differs from the synergy with ampicillin and amoxicillin. We hypothesized that
375 PBP-lipo repression might increase the permeability of the cell wall, allowing more drug to enter

376 the cell. To test this hypothesis, we measured the accumulation of calcein into *Mab*, which is
377 one proxy for cell permeability. Calcein accumulated more rapidly in PBP-lipo knockdown cells,
378 indicating that PBP-lipo increased the permeability of *Mab* cells (Supplemental Figure 14). This
379 increased permeability might lead to increased antibiotic access to the cell, thus sensitizing the
380 bacteria to the antibiotics.
381
382 When the MICs of the same 21 antibiotics tested in *Mab* were measured in the PBP-lipo
383 knockout in *Msm,* we observed no difference in the MICs (Supplemental Table 5). We also
384 measured the MICs of a subset of these antibiotics in the PBP-lipo knockout in *Mtb* and found
385 no difference in MICs between the wildtype and knockout strain (Supplemental Table 6). These
386 data suggest that PBP-lipo's unique function in *Mab's* PG synthesis network likely contributes to
387 the species' sensitivity to antibiotics when the enzyme is repressed.
388
389 **Repression of PBP-lipo sensitizes *Mab* clinical isolates to antibiotics**
390 The antibiotic experiments were conducted on the lab-adapted ATCC 19977 reference strain on
391 *Mab*, after being isolated from a knee abscess in the 1950s and propagated in the lab since
392 (3,40). Work performed in *Mtb* has demonstrated clinical isolates and lab-adapted strains
393 respond to antibiotics stressors differently (41). As a result, we tested whether knockdown of
394 PBP-lipo in *Mab* clinical isolates led to the same changes in antibiotic sensitivity as observed in
395 the reference strain.
396
397 We found that knockdown of PBP-lipo using the 3 sgRNA construct impaired cell growth in all
398 11 clinical isolates leading to a 100 to 10,000-fold difference in CFUs (Supplemental Figure
399 15A). We also confirmed that in a sub-set of the clinical isolates PBP-lipo knockdown lead to
400 elongated and inappropriately branched cells, as observed in the reference strain
401 (Supplemental Figure 15B). After confirming the PBP-lipo phenotypes in the clinical isolates, we

402 measured the MICs of ampicillin, amoxicillin, meropenem, rifampicin, and clarithromycin on
403 PBP-lipo knockdowns of the clinical isolates.
404
405 For amoxicillin and ampicillin, PBP-lipo knockdown reduced the MICs by >32 to >512-fold.
406 Meropenem served as a negative control and indeed, there was no difference in MICs between
407 uninduced and induced strains (Table 2). Finally, we observed an 8-32X fold difference in the
408 MICs for rifampicin and 8-128X fold difference in the MICs for clarithromycin (Table 3).
409 Altogether, the antibiotic sensitivity data demonstrate that the phenotypic consequences of
410 repressing PBP-lipo is not just limited to the lab-adapted reference strain, but is observed in
411 *Mab* clinical isolates as well.

412 **Discussion**

413 Developing new drugs and drug regimens against *Mab* requires a better understanding of the
414 bacterium's essential processes. This includes identifying essential *Mab* genes for further
415 characterization as potential drug targets. To do this, we generated high-density transposon
416 libraries to identify essential genes in the reference strain, *M. abscessus subsp. abscessus*
417 ATCC 19977*.* Importantly, *Mab* transposon libraries with fewer than 10,000 unique mutants
418 have been previously published, but these studies did not identify the full list of essential genes
419 in *Mab* (10,11). Recently, Rifat *et al* successfully generated high-density libraries and were the
420 first group to identify essential genes and genomic elements in the *Mab* genome (12). All
421 together, they identified 326 essential genes and compared this list to essential genes identified
422 in *Mtb* and *Mycobacterium avium.* Similar to our study, Rifat *et al* highlighted uniquely essential
423 genes in *Mab,* which they also state deserve further study as these genes could represent *Mab*
424 specific drug targets (12).

425

426 In addition to identifying essential genes in *Mab*, our study builds upon Rifat *et al's* work by
427 using CRISPRi to repress gene expression and validate predicted essential genes as required
428 for *in vitro* growth (24). Furthermore, we found that by targeting genes with multiple sgRNAs,
429 CRISPRi can achieve significant gene repression, allowing for the investigation of essential
430 genes and providing an alternative to gene knockouts. Constructing gene knockouts in *Mab* can
431 be inefficient (42); thus, CRISPRi provides a convenient tool for genetic manipulation in *Mab.*
432 Overall, the newly generated *Mab* transposon libraries can be used to determine genes required
433 for growth in a variety of conditions including infection models, biofilms, and antibiotic stress.

434

435 Both Rifat *et al's* and our TnSeq data identified PBP-lipo as the sole PBP that is essential in
436 *Mab* and non-essential in *Mtb* (12)*.* Using CRISPRi, we demonstrated the necessity of PBP-lipo
437 expression for *Mab* to maintain normal morphology and to divide properly. When PBP-lipo is

438 repressed, cells elongate, branch, and form ectopic poles. We localized PBP-lipo to the
439 subpolar regions of the cell, and as cells elongate and prepare for division, PBP-lipo localizes to
440 the septum. Furthermore, depleting PBP-lipo led to the creation of multiple Z-rings in the cell
441 and likely the aberrant start of cell division and formation of branched cells Overall, the
442 constellation of PBP-lipo knockdown phenotypes mimic septal-factor depletions observed in
443 *Msm,* which also cause cells to elongate, branch, and form ectopic poles (32). These data
444 suggest that PBP-lipo is involved with PG synthesis at the septum and that depletion of the
445 enzyme leads to dysregulated septal PG synthesis and cell division.
446
447 Given PBP-lipo's localization and effect on cell division, we propose that PBP-lipo acts as an
448 essential septal PG synthesis enzyme in *Mab.* In *Mtb* and *Msm,* this is accomplished by the
449 enzyme *pbpB*, which is essential for growth. Additionally, when *pbpB* is repressed in these
450 species, cells appear morphologically similar to the PBP-lipo knockdown in *Mab* (32,37).
451 Interestingly, PBP-lipo knockouts in both *Msm* and *Mtb* are morphologically identical to wildtype
452 cells (Supplemental Figure 7). These data underscore that biological insights from *Msm* and *Mtb*
453 should not be de-facto applied to *Mab*. We hypothesize that PBP-lipo is a member of the *Mab*
454 divisome complex, a collection of structural proteins and enzymes that coordinates cell division
455 (43). This hypothesis was supported by the co-localization of PBP-lipo with FtsZ, a key initiating
456 component of the bacterial divisome (34). Future studies are needed to determine if PBP-lipo
457 interacts with known septal factors, such as FtsQ and FtsW, whose functions in the divisome
458 have been described in *Msm* (44–46). Future work may also reveal novel PBP-lipo binding
459 factors that coordinate PG synthesis and cell division in *Mab* specifically.
460
461 Phenotypes characteristic of the PBP-lipo knockdown in *Mab* were absent in the *Mtb* and *Msm*
462 PBP-lipo knockouts. Both *Mtb* and *Msm* do not have a duplicate copy of PBP-lipo in their
463 genomes. Thus, to explain the differential essentiality of PBP-lipo across these mycobacterial

464 species, one hypothesis we explored was differences in the genetic networks of PG synthesis
465 enzymes. Construction of the PG layer is a complex process that involves a collection of
466 enzymes that work in concert to ensure proper synthesis and remodeling. Previous work has
467 shown that PG synthesis enzymes belong to genetic and spatiotemporal networks that do not
468 necessarily replicate across closely related species (36,47). Thus, while the synthetic enzymes
469 to construct the PG layer may be homologous between species, how the enzymes are
470 networked and subsequently function together may differ. We demonstrated that PBP-lipo
471 genetically interacts with *pbpB, dacB1,* and *MAB_0519*. In contrast, TnSeq on the *Msm* Δ*pbp-*
472 *lipo* strain did not reveal interactions with any other gene in the genome. This demonstrates that
473 despite being homologs, PBP-lipo in *Mab* and *Msm* are incorporated into different PG synthesis
474 networks. In *Mab,* this network renders PBP-lipo's function as essential for growth and proper
475 cell division, whereas in *Msm,* PBP-lipo is dispensable. Interestingly, in *Mtb* PBP-lipo is required
476 for normal growth in a *ponA2* knockout suggesting that PBP-lipo and PonA2 genetically interact
477 *Mtb* (36) – a genetic interaction that was not observed in *Mab*. This observation supports the
478 hypothesis that PBP-lipo is incorporated in different PG synthesis in *Mtb* as well.
479
480 While this work demonstrates the essential function of PBP-lipo for growth and division in *Mab*
481 and not in *Msm* or *Mtb,* all the experiments were performed in standard growth conditions.
482 Studies in other bacteria have demonstrated that homologous PBPs that are otherwise non-
483 essential become required under specific growth conditions. For example, in *Salmonella*, the
484 class B homolog of PBP3, PBP3-SAL, was required for cell division in acidified intraphagosomal
485 environments (48). Similarly, in *E. coli*, PBP6, which encodes a carboxypeptidase, was more
486 active at lower pH values compared to 5 other homologous carboxypeptidases (49). These
487 studies demonstrate that some PBPs become more active and their functions more required in
488 specific growth conditions. Future studies could test PBP-lipo's function under various stress

489 conditions. These experiments may elucidate a condition-specific role for PBP-lipo in *Msm* and
490 *Mtb* that differs from its central function in *Mab.*
491
492 Not only is PBP-lipo essential in *Mab,* it also genetically interacts with three other PBPs, *pbpB,*
493 *dacB1,* and *MAB_0519,* which are all hypothesized to be septal associated. PbpB is a D,D-
494 transpeptidase that performs 4,3 crosslinking reactions at the septum. In *Msm*, depleting PbpB
495 leads to cell filamentation and branching reminiscent of the *Mab* PBP-lipo knockdown
496 phenotypes (32). A potential explanation of this genetic interaction is both PbpB and PBP-lipo
497 perform 4,3-crosslinking at the *Mab* septum. In this model, repressing both enzymes would
498 dramatically reduce 4,3-crosslinking at the septum and lead to cell death. We explored this
499 model by overexpressing PbpB while strongly repressing PBP-lipo. We discovered
500 overexpressing PbpB completely reversed the growth and morphological defect of PBP-lipo
501 knockdown. This data provided evidence that PBP-lipo and PbpB have overlapping 4-3 cross-
502 linking function at the septum, and that by supplying the cell with more D,D-transpeptidation
503 activity via PbpB, the deleterious effects of PBP-lipo repression were reversed. Interestingly,
504 given that both PBP-lipo and PbpB are essential in *Mab*, the enzymes must have overlapping,
505 but distinct functional roles. Their distinct functions could be revealed by identifying unique
506 genetic or physical interactions each enzyme has with other PG synthesis enzymes. Why *Mab*
507 requires two PG 4,3 crosslinking enzymes functioning at the septum is an intriguing area of
508 future research.
509
510 The two other genes that synergized with PBP-lipo, DacB1 and MAB_0519, are both
511 hypothesized carboxypeptidases that cleave the terminal D-ala-D-ala on the pentapeptide
512 chains of PG monomers forming a tetrapeptide. This substrate is necessary for 3,3 crosslinks
513 catalyzed by L-D transpeptidases (LDTs) (50,51). Interestingly, DacB1 localizes to the septum
514 in *Mab* and has been described as septally localized in *Msm* and *Mtb* (52). In *Mab,* DacB1 also

515 co-localizes with PBP-lipo at the septum. Furthermore, the homolog of MAB_0519 in *Mtb*,
516 Rv3627c is involved in septal PG synthesis (53). Thus, we hypothesize DacB1 and MAB_0519
517 are involved in septal PG synthesis and may work with PBP-lipo to ensure proper PG synthesis
518 and remodeling at the septum. Interestingly, DacB1 and MAB_0519 are not functionally
519 redundant, given that both genes are synergistic with PBP-lipo. Further characterization of the
520 PG enzymes in *Mab* and their genetic networks will uncover species-specific nuances in *Mab*
521 PG synthesis that have the potential to be exploited for drug discovery.
522
523 Knockdown of PBP-lipo dramatically sensitized the reference *Mab* strain and 11 clinical isolates
524 to several antibiotics. The PBP-lipo knockdown was >128-fold more sensitive to the β-lactams,
525 ampicillin and amoxicillin, while other β-lactams such as like meropenem, cephalexin, ticarcillin
526 and others showed no difference in MIC. This result indicates a specific chemical-genetic
527 interaction between ampicillin/amoxicillin, and PBP-lipo. Historically, β-lactams have not been
528 used to treat *Mab* infections due to high levels of resistance and the presence of β-lactamases
529 (20). While imipenem and cefoxitin are used with some success, macrolides and
530 aminoglycosides remain the backbone of *Mab* treatment (54). Recently, studies have shown
531 dual β-lactam strategies are effective in killing *Mab* both *in vitro* and *in vivo* (55–57). These
532 synergy data suggest that understanding the specific antibiotic targets of β-lactams in *Mab*
533 would augment the design of effective dual β-lactam combinations. At the moment, effective
534 combinations are usually tested empirically with no insight into potential mechanisms (56).
535 Recently, a potential mechanism for dual-beta lactam synergy in *Mab* was uncovered by Dousa
536 *et al.* The group discovered that the novel beta-lactamase inhibitor, durlobactam, also inhibited
537 a *Mab* carboxypeptidase and by doing so, greatly enhanced *Mab* sensitivity to amoxicillin and
538 imipenem combination therapy (58). Another attempt to identify specific targets of PBP targets
539 of beta-lactams was conducted by Sayed *et al*. This group used a combination of a bocillin FL

binding assay to stain all the PBPs in *Mab* followed by proteomics to identify the targets of 12 β-lactams and 2 β-lactamases. Interestingly, in their datasets, PBP-lipo was not identified by mass spectrometry of bocillin FL-bounded PBPs (59). This further supports our hypothesis that PBP-lipo is expressed at low-levels in *Mab* and is not identifiable by bocillin FL staining under native expression conditions.

Nonetheless, our data demonstrate that using a β-lactam or small molecules that target PBP-lipo would not only kill the cell, but also potentiate β-lactams like ampicillin and amoxicillin. In addition, the permeabilizing effect of PBP-lipo inhibition would potentiate drugs by allowing more compound to enter the cell. Crucially, the observed synergy with PBP-lipo knockdown and β-lactams was not only limited to the reference strain, but also present in 11 clinical isolates of *Mab,* indicating that this synergy can be broadly targeted in *Mab* clinical isolates.

Overall, this work employed TnSeq to identify the uniquely essential gene PBP-lipo in *Mab*. We present PBP-lipo as a promising drug target given both its essentiality in *Mab* cell growth and division and its role in sensitizing *Mab* to a range of antibiotics, including commonly used and accessible antibiotics, ampicillin and amoxicillin. Future studies exploring the PBP networks of mycobacteria can expose further species-specific vulnerabilities in peptidoglycan synthesis. Finally, identifying chemical inhibitors of PBP-lipo may help form the foundation for new treatments against this emerging and difficult to treat pathogen.

560 **Materials and Methods**
561

562 A full list of the strains, plasmids, and primers is available in Supplemental Tables 7, 8, and 9
563 respectively.

564
565 **Bacterial Strains and Culture Conditions:** All *Mab* and *Mtb* strains were grown shaking at
566 37°C in liquid 7H9 media consisting of Middlebrook 7H9 salts with 0.2% glycerol, 0.85 g/L NaCl,
567 OADC (oleic acid, 5 g/L albumin, 2 g/L dextrose, 0.003 g/L catalase), and 0.05% Tween80. *Mab*
568 and *Mtb* were plated on Middlebrook 7H10 agar supplemented with 0.5% glycerol. *Msm* was
569 grown shaking at 37°C in liquid on 7H9 media consisting of Middlebrook 7H9 salts with 0.2%
570 glycerol, 0.85 g/L NaCl, ADC, and 0.05% Tween80 and plated on LB agar. Antibiotic selection
571 concentrations for *Mab* cultures were kanamycin 50 µg/µl and zeocin 100 µg/µl. For transposon
572 mutant selection, 100 µg/ml of kanamycin was used. Antibiotic selection concentrations for *Msm*
573 and *Mtb* cultures were kanamycin 25 µg/µl, zeocin 20 µg/µl, and gentamicin 5 µg/µl. For *E. coli*
574 (TOP10, XL1-Blue and DH5α), all antibiotic concentrations were twice those of the
575 concentrations used for *Msm* and *Mtb*. Induction of all CRISPRi plasmids was performed with
576 500 ng/ul anhydrous tetracycline (ATc).

577

578 **Strain Construction**

579 *Construction of 0, 1, 2, 3 sgRNA PBP-lipo knockdown strains and PBP-lipo complement strains*
580 To build the 0 sgRNA (empty sgRNA) *Mab* strain, we transformed the pCT296 vector containing
581 an empty sgRNA into *Mab.* To build the 1, 2, and 3 sgRNA strains, first we built individual
582 CRISPRi plasmids containing single sgRNAs that targeted PBP-lipo. These plasmids were cr25,
583 cr26, and cr56. We then designed primers that amplified the sgRNA targeting region with the
584 appropriate flanking sequences and performed Golden Gate cloning to combine the inserts into
585 one vector. This method was previously described by Rock et al (24). For the 1 sgRNA strain,
586 we transformed cr25 into the *Mab* strain. For the 2 sgRNA, we transformed the vector pCRC1,

587 which contained the cr25 and cr26 sgRNAs on one backbone. Finally, for the 3 sgRNA strain we
588 transformed pCRC2, which contained the cr25, cr26, and cr56 sgRNAs on one backbone.
589 To build the PBP-lipo complement strain, we designed primers to amplify PBP-lipo with modified
590 protospacer adjacent motif (PAM) sequences that were no longer homologous to the 1 and 2
591 sgRNAs. This recoded PBP-lipo was then cloned into a constitutive expression vector resulting
592 in the pCA323 construct, which was transformed into the 2 sgRNA strain. The catalytically dead
593 mutant version of the recoded PBP-lipo was generated by using primers to generate the S364A
594 mutation. This engineered PBP-lipo was cloned into a constitutive expression vector and the
595 resulting construct, pCA324 was transformed into the 2 sgRNA strain.
596
597 *Msm* and *Mtb* ΔPBP-lipo strains
598 To generate PBP-lipo knockout mutants in *Msm* and *Mtb,* we used a recombineering approach
599 to replace the endogenous copy of the gene with a zeocin resistance cassette as previously
600 described (60). First, 500 base pairs of upstream and downstream sequence surrounding PBP-
601 lipo (*Rv2864c* and *MSMEG_2584c*) were amplified by PCR KOD XtremeTM Hot Start DNA
602 polymerase (EMD Millipore, Billerica, MA). These flanking regions were amplified with overlaps
603 for the zeocin resistance cassette. The 2 flanking regions and zeocin resistance cassette were
604 then assembled via isothermal assembly (61) into a single construct, which was then amplified
605 by PCR. Each deletion construct was transformed into either *Mtb* or *Msm* expressing inducible
606 copies of RecET (62). The resulting colonies were screened for the PBP-lipo deletion by PCR.
607
608 *PBP-lipo$_{Mab}$-strep expression strain*
609 PBP-lipo$_{Mab}$ was amplified using primers that added a C-terminal strep tag to the protein. The
610 resulting insert was Gibson stitched to the vector backbone that drove expression of PBP-
611 lipo$_{Mab}$-strep from the constitutively active MOP promoter.
612

613 *mRFP-PBP-lipo$_{Mab}$*

614 We amplified PBP-lipo$_{Mab}$ in two fragments. The first fragment contained the N-terminal signal
615 sequence of PBP-lipo. The second fragment contained the remainder of the protein. We then
616 amplified mRFP with overhangs that were compatible with the two fragments of PBP-lipo. The
617 resulting three fragments were Gibson assembled to a vector backbone that constitutively drove
618 expression of the mRFP-PBP-lipo$_{Mab}$ fusion protein. A gly-gly-ser-gly-ser-gly linker was used in
619 between mRFP and the two fragments of PBP-lipo.

620

621 *DacB1-GFP-strep*

622 DacB1 lacking a stop codon was amplified along with GFP containing overlaps with DacB1 and
623 a gly-gly-ser linker. The two fragments were Gibson assembled to a vector backbone that
624 constitutively drove expression of the DacB1-GFP-strep fusion protein.

625

626 *ftsZ-mNeonGreen & DacB1-mNeonGreen*

627 ftsZ and DacB1 were amplified along with mNeonGreen containing a gly-gly-ser linker. Each
628 gene and its corresponding overlapping mNeonGreen fragment were Gibson assembled to a
629 vector that constitutively drove expression from the weak promoter iMyc.

630

631 *natP-GFP-ftsZ*

632 To express FtsZ off its natural promoter, 300bp of sequence upstream of the FtsZ start codon
633 was amplified and Gibson assembled with 2 additional fragments corresponding to GFP with a
634 gly-gly-ser linker and FtsZ. The resulting vector was an N-terminal GFP-FtsZ fusion expressed
635 off the FtsZ natural promoter.

636

637 **Growth Curve:** *Mab, Msm,* and *Mtb* cultures were grown to log phase and diluted to OD600
638 0.05. Growth curves were performed in a 96 well format at 37°C with shaking. OD600 was
639 measured every 15 min for 24-72 hr using the TECAN plate reader
640
641 **Colony Forming Units:** *Mab* and *Msm* cultures were grown to mid-log phase and then serially
642 diluted in their respective media in 96 well plates. Dilutions were then spot plated onto solid
643 media +/- 500 ng/ul ATc. Plates were incubated at 37°C for 4 days *(Mab)* or 3 days *(Msm)*. After
644 incubation, the resulting CFUs were calculated by counting the number of colonies at the
645 appropriate dilution. The fraction survivability was calculated as CFUs +ATc / -ATc.
646
647 **Minimum Inhibitory Concentration Determination:** *Mab, Msm,* and *Mtb* were grown to mid-
648 log phase and diluted to an OD600 = 0.003 in each well of non-treated 96-well plates (Genesee
649 Scientific) containing 100 µL of antibiotic serially diluted in 7H9 + OADC + 5 µg/mL clavulanate
650 (Sigma Aldrich). For MICs on *Mab* knockdown cells, cultures were induced for knockdown 18 hr
651 prior with 500 ng/ul ATc. Wells with knockdown bacteria also contained 500 ng/ul ATc. *Msm*
652 media contained ADC rather than OADC. Cells were incubated with drug at 37°C with shaking
653 for 1 day *(Mab, Msm)* or 7 days *(Mtb)*. Afterwards, 0.002% resazurin diluted in ddH_2O (Sigma
654 Aldrich) was added to each well. Plates were then incubated for 24 hr. MICs were determined
655 by the concentration of antibiotic that turned wells blue signifying no metabolic activity (63).
656
657 **Generation of Transposon Libraries:** To create transposon mutant libraries of *Mab* ATCC
658 19977 and *Msm* (wildtype and ΔPBP-lipo), 100 ml of bacterial cultures were grown to an OD600
659 of 1.5 – 2.0. For *Mab*, cultures were grown in biological triplicate. For *Msm*, the wildtype strain
660 was grown in duplicate while one replicate of the ΔPBP-lipo strain was grown. The cells were
661 then washed twice with 50 ml of MP Buffer (50mM Tris-HCl pH 7.5, 150 mM NaCl, 10 mM
662 $MgSO_4$, 2 mM $CaCl_2$) and resuspended in 1/10th the culture volume in MP Buffer. Afterwards, 2

663 x 10^{11} pfu of temperature sensitive φMycoMarT7 phage carrying the Himar1 transposon were
664 added to bacteria. Phage and bacterial cultures were incubated at 37°C for 4 hr with shaking.
665 The transduced cultures were spun down at RT 4000 rpm for 10 min and resuspended in 12 ml
666 of PBS-Tween. The cultures were then tittered by plating on 7H10 plates (*Mab)* or LB *(Msm)*
667 supplemented with kanamycin 100 µg/µml *(Mab)* or 20 µg/µl *(Msm)* before freezing the aliquots
668 for future plating. After determining the titer, 150,000 bacterial mutants of each transduced
669 culture were plated onto kanamycin selective plates and grown for 4 days at 37°C. The resulting
670 mutant libraries were harvested and stored in aliquots with 7H9 + 10% glycerol at -80°C.
671
672 **Genomic DNA Extraction:** To prep libraries for sequencing, we isolated the gDNA of the
673 mutant libraries using a bead-beating protocol developed in the lab. 2-6 ml of transposon mutant
674 libraries were thawed and spun down to remove excess glycerol in the sample. Pellets were
675 then resuspended in TE Buffer (10 mM Tris HCl pH 7.4, 1 mM EDTA pH8) and placed in bead-
676 beating tubes with 600 µl of 25:24:1 phenol:chloroform:isoamyl alcohol. The samples were then
677 bead-beat 4X for 45 s at 4000 rpm. Samples were cooled on ice for 45 s between each
678 successive bead-beat round. After bead-beating, the samples were spun down for 10 min at
679 13,000 rpm. The supernatant was transferred to a new falcon tube and incubated with 1:1
680 volume phenol:chloroform for 1 hr rocking. Samples were then spun down in MaXtract High
681 Density phase-lock tubes (Qiagen) at 1500 g for 5 min. This separated the aqueous and organic
682 layers. Afterwards, ½ volume of chloroform was added to the tube and the contents were spun
683 down at 1500 g for 5 min. The aqueous phase was transferred to a new tube and RNAse A
684 (Thermo Fisher) was added to a final concentration of 25 µg/µl. The tubes were incubated at
685 37°C for 1 hr with shaking. Finally, the supernatant was washed with 1:1 volume of phenol-
686 chloroform followed by ½ volume of chloroform. The aqueous phase was transferred to a new
687 tube and genomic DNA was precipitated with 1 volume of isopropanol alcohol and 1/10th
688 volume of 3 M sodium acetate pH 5.2. The library gDNA was washed twice with fresh 70%

689 ethanol and resuspended in nuclease free ddH_2O. This protocol consistently generated high
690 yields of *Mab* gDNA.
691
692 **Transposon sequencing, mapping, and analysis:** Sequencing libraries were prepared from
693 the extracted gDNA by amplifying chromosomal-transposon junctions following the protocol as
694 described by Long et al, 2015 (21). These amplicons were then sequenced using the Illumina
695 Hi-Seq platform. The resulting reads were mapped onto the *Mab* or *Msm* genomes. The data
696 were analyzed using the TRANSIT pipeline (23). Insertion counts at each TA site were
697 normalized using TTR and averaged across replicates. Essentiality categories of genes were
698 determined by the Hidden Markov Model (HMM) algorithm in TRANSIT. Resampling analysis
699 was used to compare insertion accounts between genes in the wildtype and ΔPBP-lipo *Msm*
700 strains.
701
702 **Cloning of CRISPRi Constructs:** To clone sgRNAs onto the CRISPRi vector backbone,
703 complimentary targeting oligos were annealed and ligated (T4 DNA ligase, NEB) into the BsmBI
704 digested CRISPRi vector backbone. To clone multiple sgRNAs into the same vector, the
705 promoter, sgRNA handle, and sgRNA sequences were amplified with the appropriate flanking
706 sequences to perform Golden Gate cloning using the SapI cloning site in the CRISPRi vector
707 (24). All cloning was performed using DH5α cells and sequences were verified before
708 transformation into *Mab* and *Msm.*
709
710 **Transformation of *Mab*:** To generate electrocompetent *Mab* cells, 50 ml of *Mab* cultures were
711 grown to mid-log phase. Cells were spun down at 4000 rpm for 10 min and washed twice with
712 pre-chilled 10% glycerol. Cell pellets were resuspended in 1/100th of the starting volume and
713 kept on ice for immediate use or stored at -80°C for future use. For transformations ~100 ng of
714 plasmid DNA was incubated with electro-competent cells for 5 min before electroporation using

715 the settings: 2500 V, 125 Ω, 25 µF. Afterwards, cells were recovered in 1 ml of 7H10 with OADC
716 without selection for 3 hr at 37°C with shaking. Cells were then plated on 7H10 with the
717 appropriate selection marker and incubated for 4 days at 37°C.
718
719 **Microscopy and Image Analysis:** All imaging was performed on an inverted Nikon TI-E
720 microscope at 60X and 100X magnification. For PBP-lipo knockdown experiments, cultures
721 were induced for knockdown with 500 ng/ul ATc for 18 hr prior to imaging. All *Mab* cultures were
722 fixed with 7H9 + 3% paraformaldehyde (PFA) for 1 hr and resuspended in PBS + 0.05%
723 Tween80 prior to imaging. Cellular features including cell length, width, and fluorescence signal
724 were analyzed using the MOMIA and GEMATRIA image analysis pipelines developed in the lab
725 (35).
726
727 **Fluorescent D-Amino Acid Staining:** NADA (3-[(7-Nitro-2,1,3-benzoxadiazol-4-yl)amino]-D-
728 alanine hydrochloride) was synthesized by Tocris following the published protocol (31). To stain
729 *Mab* with NADA, 0.1 mM of FDAA was added to 1 ml of exponentially growing cells and
730 incubated for 3 min before washing in warm 7H9 twice. For *Mab* imaging, after the second
731 wash, cells were fixed in 7H9 + 3% paraformaldehyde for 1 hr. The PFA was then washed off
732 and cells were resuspended in PBS + 0.05% Tween80 prior to imaging.
733
734 **RNA Extraction and RT-qPCR:** For each strain, cultures were grown in biological triplicate to
735 mid-log phase and then diluted back in +/- 500 ng/ml ATc and grown for 18 hr to achieve target
736 knockdown. Afterwards, 2 OD 600 equivalents of cells from each culture were harvested by
737 centrifugation, resuspended in TRIzol (Thermo Fisher), and lysed by bead beating (Lysing
738 Matrix B, MP Biomedicals). Total RNA was extracted using the RNA miniprep (Zymo Research).
739 Residual genomic DNA was digested with TURBO DNase (Ambion), and samples were cleaned
740 with RNA clean-up columns (Zymo Research). cDNA was prepared using random hexamers

741 following manual instructions (Life Technologies Superscript IV). Alkaline hydrolysis was then
742 used to remove RNA. cDNA was purified by spin column (Qiagen) and then quantified by real-
743 time quantitative PCR (RT–qPCR) on a Viia7 light cycler (Applied Biosystems) using iTaq
744 Universal SYBR Green Supermix (BioRad). All qPCR primer pairs were confirmed to be >95%
745 efficient. The masses of cDNA used were experimentally validated to be within the linear
746 dynamic range of the assay. Signals were normalized to the *sigA* (*MAB_3009*) transcript and
747 quantified by the ΔΔCt method. Error bars are standard deviations from three biological
748 replicates.
749
750 **Bocillin FL staining:** *Mab* cultures were grown to mid-log phase and 10 OD units of bacteria
751 were spun down and resuspended in 1ml of fresh 7H9 media with 5 µg/ml of clavulanate.
752 Bocillin-BODIPY or FITC were added to cultures to a final concentration of 10 µM. Cells were
753 then incubated at 37°C for 2.5 hr, with aluminum wrapping to prevent light exposure. After
754 labeling, cells are washed with PBS + 0.05% Tween80 three times and resuspended in 200 µl
755 of lysis buffer (50 mM Tris-HCl pH = 7.4, 50 mM NaCl, protease inhibitor (Roche)). Samples
756 were bead beat 4X at 4000 rpm for 1 min with 1 min of rest on ice in between rounds of bead-
757 beats. $CaCl_2$ was added to a final concentration of 1 mM along with 4U of DNAse I and 10
758 mg/ml of fresh lysozyme. Samples were incubated at 37°C for 30 min. Afterwards, supernatants
759 were normalized by A280 protein concentration, diluted with 6X Laemmli buffer, and run on 4%–
760 12% NuPAGE Bis Tris precast gels (Life Technologies). To visualize fluorescence, we used a
761 BioRad Gel Doc system. To detect the presence of PBP-lipo-strep, we performed a Western
762 Blot. Membranes were blotted with rabbit α-Strep (GenScript) at 1:1000 in TBST + 3% BSA.
763
764 **Calcein Staining:** For each strain, cultures were grown in biological triplicate to mid-log phase
765 and diluted back in +/- 500 ng/ml ATc and grown for 18 hr to achieve target knockdown.
766 Afterwards, 3 OD units of bacteria were washed twice with PBS + 0.05% Tween80. Cells were

767 resuspended in PBS + 0.05% Tween80 and 100 µl of cells at OD600 = 0.4 was added to 96
768 well plates. The plates were incubated in the plate reader for 30 min at 37°C with shaking.
769 Afterwards, calcein was added at a final concentration of 1 µg/ml. Fluorescence signal was
770 measured every minute using the Tecan plate reader.

Acknowledgements

This project was funded by the generous support of the Paul and Daisy Soros Foundation, the NIH/NIAID F31 Predoctoral Fellowship award number F31AI149932, and award Number T32GM007753 from the National Institute of General Medical Sciences. The content is solely the responsibility of the authors and does not represent the official views of the National Institute of General Medical Sciences or the National Institutes of Health.

References

1. Bryant JM, Grogono DM, Rodriguez-Rincon D, Everall I, Brown KP, Moreno P, et al. Emergence and spread of a human-transmissible multidrug-resistant nontuberculous mycobacterium. Science. 2016 Nov 11;354(6313):751–7.

2. Primm TP, Lucero CA, Falkinham JO. Health impacts of environmental mycobacteria. Clin Microbiol Rev. 2004 Jan;17(1):98–106.

3. Johansen MD, Herrmann JL, Kremer L. Non-tuberculous mycobacteria and the rise of Mycobacterium abscessus. Nat Rev Microbiol. 2020 Feb 21;1–16.

4. Nessar R, Cambau E, Reyrat JM, Murray A, Gicquel B. Mycobacterium abscessus: a new antibiotic nightmare. J Antimicrob Chemother. 2012 Apr;67(4):810–8.

5. Pang H, Li G, Wan L, Jiang Y, Liu H, Zhao X, et al. In vitro drug susceptibility of 40 international reference rapidly growing mycobacteria to 20 antimicrobial agents. Int J Clin Exp Med. 2015;8(9):15423–31.

6. Jarand J, Levin A, Zhang L, Huitt G, Mitchell JD, Daley CL. Clinical and microbiologic outcomes in patients receiving treatment for Mycobacterium abscessus pulmonary disease. Clin Infect Dis Off Publ Infect Dis Soc Am. 2011 Mar 1;52(5):565–71.

7. Bryant JM, Brown KP, Burbaud S, Everall I, Belardinelli JM, Rodriguez-Rincon D, et al. Stepwise pathogenic evolution of Mycobacterium abscessus. Science. 2021 Apr 30;372(6541):eabb8699.

8. van Opijnen T, Camilli A. Transposon insertion sequencing: a new tool for systems-level analysis of microorganisms. Nat Rev Microbiol. 2013 Jul;11(7):435–42.

9. DeJesus MA, Gerrick ER, Xu W, Park SW, Long JE, Boutte CC, et al. Comprehensive Essentiality Analysis of the Mycobacterium tuberculosis Genome via Saturating Transposon Mutagenesis. mBio. 2017 Jan 17;8(1):e02133-16.

10. Foreman M, Gershoni M, Barkan D. A Simplified and Efficient Method for Himar-1 Transposon Sequencing in Bacteria, Demonstrated by Creation and Analysis of a Saturated Transposon-Mutant Library in Mycobacterium abscessus. mSystems. 2020 Oct 20;5(5):e00976-20.

11. Laencina L, Dubois V, Le Moigne V, Viljoen A, Majlessi L, Pritchard J, et al. Identification of genes required for Mycobacterium abscessus growth in vivo with a prominent role of the ESX-4 locus. Proc Natl Acad Sci U S A. 2018 30;115(5):E1002–11.

12. Rifat D, Chen L, Kreiswirth BN, Nuermberger EL. Genome-Wide Essentiality Analysis of Mycobacterium abscessus by Saturated Transposon Mutagenesis and Deep Sequencing. mBio. 2021 Jun 15;e0104921.

13. Wong EB, Cohen KA, Bishai WR. Rising to the challenge: New therapies for tuberculosis. Vol. 21, Trends in Microbiology. 2013. p. 493–501.

14. Bhat ZS, Rather MA, Maqbool M, Lah HU, Yousuf SK, Ahmad Z. Cell wall: A versatile fountain of drug targets in Mycobacterium tuberculosis. Vol. 95, Biomedicine and Pharmacotherapy. 2017. p. 1520–34.

15. Jarlier V, Nikaido H. Mycobacterial cell wall: Structure and role in natural resistance to antibiotics. FEMS Microbiol Lett. 1994 Oct 1;123(1–2):11–8.

817 16. Nasiri MJ, Haeili M, Ghazi M, Goudarzi H, Pormohammad A, Imani Fooladi AA, et al. New Insights in
818 to the Intrinsic and Acquired Drug Resistance Mechanisms in Mycobacteria. Front Microbiol. 2017
819 Apr 25;8:681.

820 17. Kieser KJ, Rubin EJ. How sisters grow apart: Mycobacterial growth and division. Vol. 12, Nature
821 Reviews Microbiology. Nature Publishing Group; 2014. p. 550–62.

822 18. Arora D, Chawla Y, Malakar B, Singh A, Nandicoori VK. The transpeptidase PbpA and noncanonical
823 transglycosylase RodA of Mycobacterium tuberculosis play important roles in regulating bacterial
824 cell lengths. J Biol Chem. 2018 Apr 27;293(17):6497–516.

825 19. Slayden RA, Belisle JT. Morphological features and signature gene response elicited by inactivation
826 of FtsI in Mycobacterium tuberculosis. J Antimicrob Chemother. 2009 Mar 1;63(3):451–7.

827 20. Soroka D, Dubée V, Soulier-Escrihuela O, Cuinet G, Hugonnet JE, Gutmann L, et al.
828 Characterization of broad-spectrum Mycobacterium abscessus class A β-lactamase. J Antimicrob
829 Chemother. 2014 Mar;69(3):691–6.

830 21. Long JE, DeJesus M, Ward D, Baker RE, Ioerger T, Sassetti CM. Identifying essential genes in
831 Mycobacterium tuberculosis by global phenotypic profiling. Methods Mol Biol Clifton NJ.
832 2015;1279:79–95.

833 22. Choudhery S, Brown AJ, Akusobi C, Rubin EJ, Sassetti CM, Ioerger TR. Modeling Site-Specific
834 Nucleotide Biases Affecting Himar1 Transposon Insertion Frequencies in TnSeq Data Sets.
835 mSystems. 2021 Oct 26;6(5):e0087621.

836 23. DeJesus MA, Ambadipudi C, Baker R, Sassetti C, Ioerger TR. TRANSIT--A Software Tool for Himar1
837 TnSeq Analysis. PLoS Comput Biol. 2015 Oct;11(10):e1004401.

838 24. Rock JM, Hopkins FF, Chavez A, Diallo M, Chase MR, Gerrick ER, et al. Programmable
839 transcriptional repression in mycobacteria using an orthogonal CRISPR interference platform. Nat
840 Microbiol. 2017 Feb 6;2(4):1–9.

841 25. Peters JM, Koo BM, Patino R, Heussler GE, Hearne CC, Qu J, et al. Enabling genetic analysis of
842 diverse bacteria with Mobile-CRISPRi. Nat Microbiol. 2019 Feb;4(2):244–50.

843 26. Caro F, Place NM, Mekalanos JJ. Analysis of lipoprotein transport depletion in Vibrio cholerae using
844 CRISPRi. Proc Natl Acad Sci. 2019 Aug 20;116(34):17013–22.

845 27. Zhao G, Meier TI, Kahl SD, Gee KR, Blaszczak LC. BOCILLIN FL, a sensitive and commercially
846 available reagent for detection of penicillin-binding proteins. Antimicrob Agents Chemother. 1999
847 May;43(5):1124–8.

848 28. Rezwan M, Grau T, Tschumi A, Sander P. Lipoprotein synthesis in mycobacteria. Microbiology. 2007
849 Mar 1;153(3):652–8.

850 29. Armbruster KM, Meredith TC. Enrichment of Bacterial Lipoproteins and Preparation of N-terminal
851 Lipopeptides for Structural Determination by Mass Spectrometry. JoVE J Vis Exp. 2018 May
852 21;(135):e56842.

853 30. Young DB, Garbe TR. Lipoprotein antigens ofMycobacterium tuberculosis. Res Microbiol. 1991 Jan
854 1;142(1):55–65.

855 31. Kuru E, Tekkam S, Hall E, Brun YV, Van Nieuwenhze MS. Synthesis of fluorescent D-amino acids
856 and their use for probing peptidoglycan synthesis and bacterial growth in situ. Nat Protoc. 2015
857 Jan;10(1):33–52.

858 32. Wu KJ, Zhang J, Baranowski C, Leung V, Rego EH, Morita YS, et al. Characterization of Conserved
859 and Novel Septal Factors in Mycobacterium smegmatis. J Bacteriol. 2018 15;200(6).

860 33. Baranowski C, Welsh MA, Sham LT, Eskandarian HA, Lim HC, Kieser KJ, et al. Maturing
861 Mycobacterium smegmatis peptidoglycan requires non-canonical crosslinks to maintain shape.
862 eLife. 2018 16;7.

863 34. Adams DW, Errington J. Bacterial cell division: assembly, maintenance and disassembly of the Z
864 ring. Nat Rev Microbiol. 2009 Sep;7(9):642–53.

865 35. Zhu J, Wolf ID, Dulberger CL, Won HI, Kester JC, Judd JA, et al. Spatiotemporal localization of
866 proteins in mycobacteria. Cell Rep. 2021 Dec;37(13):110154.

867 36. Kieser KJ, Baranowski C, Chao MC, Long JE, Sassetti CM, Waldor MK, et al. Peptidoglycan
868 synthesis in Mycobacterium tuberculosis is organized into networks with varying drug susceptibility.
869 Proc Natl Acad Sci U S A. 2015 Oct 20;112(42):13087–92.

870 37. Slayden RA, Belisle JT. Morphological features and signature gene response elicited by inactivation
871 of FtsI in Mycobacterium tuberculosis. J Antimicrob Chemother. 2009 Mar;63(3):451–7.

872 38. Wissel MC, Weiss DS. Genetic Analysis of the Cell Division Protein FtsI (PBP3): Amino Acid
873 Substitutions That Impair Septal Localization of FtsI and Recruitment of FtsN. J Bacteriol. 2004
874 Jan;186(2):490–502.

875 39. Datta P, Dasgupta A, Singh AK, Mukherjee P, Kundu M, Basu J. Interaction between FtsW and
876 penicillin-binding protein 3 (PBP3) directs PBP3 to mid-cell, controls cell septation and mediates the
877 formation of a trimeric complex involving FtsZ, FtsW and PBP3 in mycobacteria. Mol Microbiol.
878 2006 Dec;62(6):1655–73.

879 40. Tortoli E, Kohl TA, Brown-Elliott BA, Trovato A, Leão SC, Garcia MJ, et al. Emended description of
880 Mycobacterium abscessus, Mycobacterium abscessus subsp. abscessus and
881 Mycobacteriumabscessus subsp. bolletii and designation of Mycobacteriumabscessus subsp.
882 massiliense comb. nov. Int J Syst Evol Microbiol. 2016 Nov;66(11):4471–9.

883 41. Allison F. Carey, Rock JM, Krieger IV, Chase MR, Fernandez-Suarez M, Gagneux S, et al. TnSeq of
884 Mycobacterium tuberculosis clinical isolates reveals strain-specific antibiotic liabilities. PLOS
885 Pathog. 2018 Mar 5;14(3):e1006939.

886 42. Medjahed H, Reyrat JM. Construction of Mycobacterium abscessus defined glycopeptidolipid
887 mutants: comparison of genetic tools. Appl Environ Microbiol. 2009 Mar;75(5):1331–8.

888 43. Kieser KJ, Rubin EJ. How sisters grow apart: mycobacterial growth and division. Nat Rev Microbiol.
889 2014 Aug;12(8):550–62.

890 44. Datta P, Dasgupta A, Singh AK, Mukherjee P, Kundu M, Basu J. Interaction between FtsW and
891 penicillin-binding protein 3 (PBP3) directs PBP3 to mid-cell, controls cell septation and mediates the
892 formation of a trimeric complex involving FtsZ, FtsW and PBP3 in mycobacteria. Mol Microbiol.
893 2006 Dec;62(6):1655–73.

894 45. Rajagopalan M, Maloney E, Dziadek J, Poplawska M, Lofton H, Chauhan A, et al. Genetic evidence
895 that mycobacterial FtsZ and FtsW proteins interact, and colocalize to the division site in
896 Mycobacterium smegmatis. FEMS Microbiol Lett. 2005 Sep 1;250(1):9–17.

897 46. Datta P, Dasgupta A, Bhakta S, Basu J. Interaction between FtsZ and FtsW of Mycobacterium
898 tuberculosis *. J Biol Chem. 2002 Jul 12;277(28):24983–7.

899 47. Botella H, Yang G, Ouerfelli O, Ehrt S, Nathan CF, Vaubourgeix J. Distinct Spatiotemporal Dynamics
900 of Peptidoglycan Synthesis between Mycobacterium smegmatis and Mycobacterium tuberculosis.
901 mBio. 2017 12;8(5).

902 48. Castanheira S, Cestero JJ, Rico-Pérez G, García P, Cava F, Ayala JA, et al. A Specialized
903 Peptidoglycan Synthase Promotes Salmonella Cell Division inside Host Cells. mBio. 2017 Dec
904 19;8(6):e01685-17.

905 49. Peters K, Kannan S, Rao VA, Biboy J, Vollmer D, Erickson SW, et al. The Redundancy of
906 Peptidoglycan Carboxypeptidases Ensures Robust Cell Shape Maintenance in Escherichia coli.
907 mBio. 2016 Jun 21;7(3):e00819-16.

908 50. Ghosh AS, Chowdhury C, Nelson DE. Physiological functions of D-alanine carboxypeptidases in
909 Escherichia coli. Trends Microbiol. 2008 Jul 1;16(7):309–17.

910 51. Ealand CS, Asmal R, Mashigo L, Campbell L, Kana BD. Characterization of putative DD-
911 carboxypeptidase-encoding genes in Mycobacterium smegmatis. Sci Rep. 2019 Mar 26;9(1):5194.

912 52. Gorla P, Plocinska R, Sarva K, Satsangi AT, Pandeeti E, Donnelly R, et al. MtrA Response Regulator
913 Controls Cell Division and Cell Wall Metabolism and Affects Susceptibility of Mycobacteria to the
914 First Line Antituberculosis Drugs. Front Microbiol. 2018;9:2839.

915 53. Zhang W, Li S, Ma L, Ding W, Xu Y. Identification of a novel carboxypeptidase encoded by Rv3627c
916 that plays a potential role in mycobacteria morphology and cell division. Enzyme Microb Technol.
917 2019 Jul 1;126:32–40.

918 54. Novosad SA, Beekmann SE, Polgreen PM, Mackey K, Winthrop KL. Treatment of Mycobacterium
919 abscessus Infection. Emerg Infect Dis. 2016 Mar;22(3):511–4.

920 55. Story-Roller E, Maggioncalda EC, Lamichhane G. Synergistic Efficacy of β-Lactam Combinations
921 against Mycobacterium abscessus Pulmonary Infection in Mice. Antimicrob Agents Chemother.
922 2019;63(8).

923 56. Pandey R, Chen L, Manca C, Jenkins S, Glaser L, Vinnard C, et al. Dual β-Lactam Combinations
924 Highly Active against Mycobacterium abscessus Complex In Vitro. mBio. 2019 Feb
925 12;10(1):e02895-18.

926 57. Lopeman RC, Harrison J, Rathbone DL, Desai M, Lambert PA, Cox JAG. Effect of Amoxicillin in
927 combination with Imipenem-Relebactam against Mycobacterium abscessus. Sci Rep. 2020 Jan
928 27;10(1):928.

929 58. Dousa KM, Nguyen DC, Kurz SG, Taracila MA, Bethel CR, Schinabeck W, et al. Inhibiting
930 Mycobacterium abscessus Cell Wall Synthesis: Using a Novel Diazabicyclooctane β-Lactamase
931 Inhibitor To Augment β-Lactam Action. mBio. 2022 Jan 25;e0352921.

932 59. Sayed ARM, Shah NR, Basso KB, Kamat M, Jiao Y, Moya B, et al. First Penicillin-Binding Protein
933 Occupancy Patterns for 15 β-Lactams and β-Lactamase Inhibitors in Mycobacterium abscessus.
934 Antimicrob Agents Chemother. 2020 Dec 16;65(1):e01956-20.

935 60. Boutte CC, Baer CE, Papavinasasundaram K, Liu W, Chase MR, Meniche X, et al. A cytoplasmic
936 peptidoglycan amidase homologue controls mycobacterial cell wall synthesis. Laub M, editor. eLife.
937 2016 Jun 15;5:e14590.

938 61. Gibson DG, Young L, Chuang RY, Venter JC, Hutchison CA, Smith HO. Enzymatic assembly of DNA
939 molecules up to several hundred kilobases. Nat Methods. 2009 May;6(5):343–5.

940 62. Murphy KC, Papavinasasundaram K, Sassetti CM. Mycobacterial recombineering. Methods Mol Biol
941 Clifton NJ. 2015;1285:177–99.

942 63. Kieser KJ, Boutte CC, Kester JC, Baer CE, Barczak AK, Meniche X, et al. Phosphorylation of the
943 Peptidoglycan Synthase PonA1 Governs the Rate of Polar Elongation in Mycobacteria. PLOS
944 Pathog. 2015 Jun 26;11(6):e1005010.

945

Figures and Legends

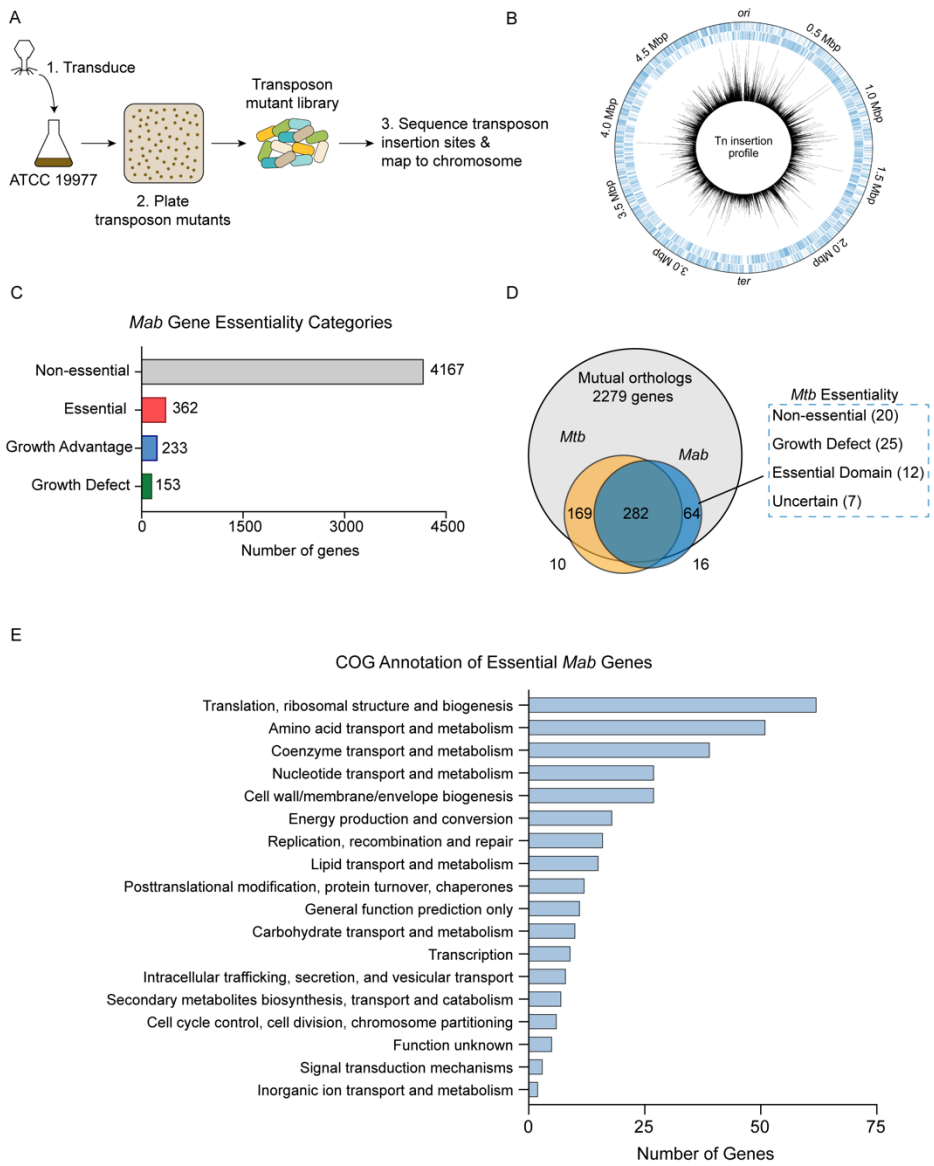

Figure 1. **Overview of TnSeq Analysis. (A)** Schematic of TnSeq protocol. Phage carrying Himar1 transposon was used to transduce *Mab subsp. abscessus* ATCC 19977 cultures. Over 51,000 independent transposon mutants were generated across three libraries **(B)** Location of transposon insertions in *Mab* genome. Black lines represent the average number of transposon insertions per gene across the three replicates. **(C)** Breakdown of gene essentiality categories as determined by the Hidden Markov Model (HMM) in TRANSIT **(D)** Essentiality comparison of mutual orthologs between *Mab* and *Mtb*. **(E)** Clusters of Orthologous Group (COG) categories of essential genes in *Mab*.

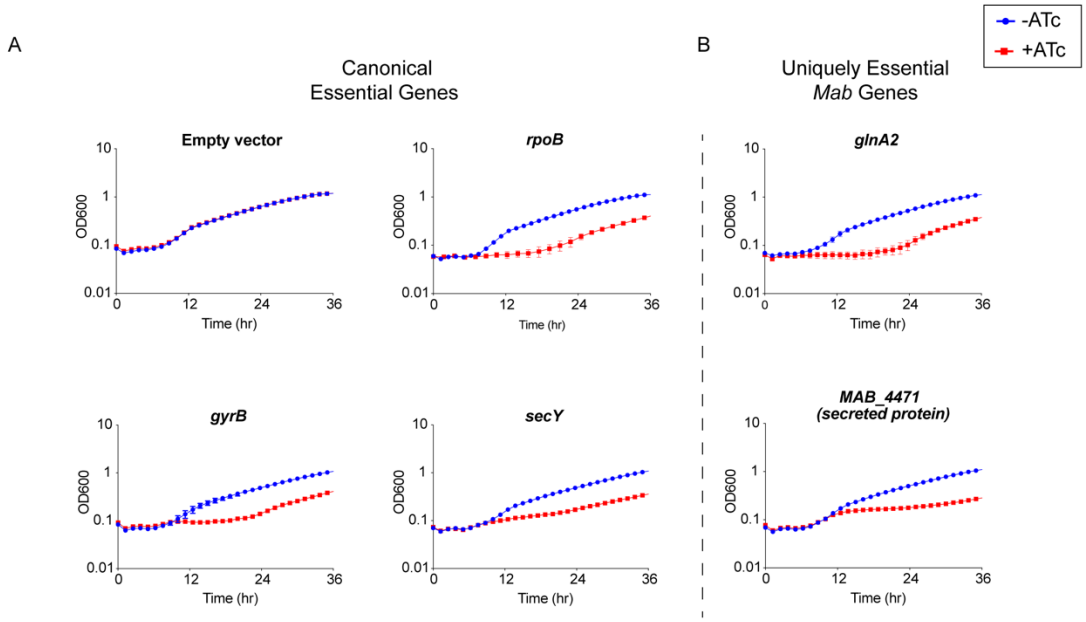

Figure 2. Validation of Essential Genes. (A) Growth curve of *Mab* strains with sgRNAs targeting canonical essential genes. **(B)** Growth curve of *Mab* strains with sgRNAs targeting uniquely essential *Mab* genes.

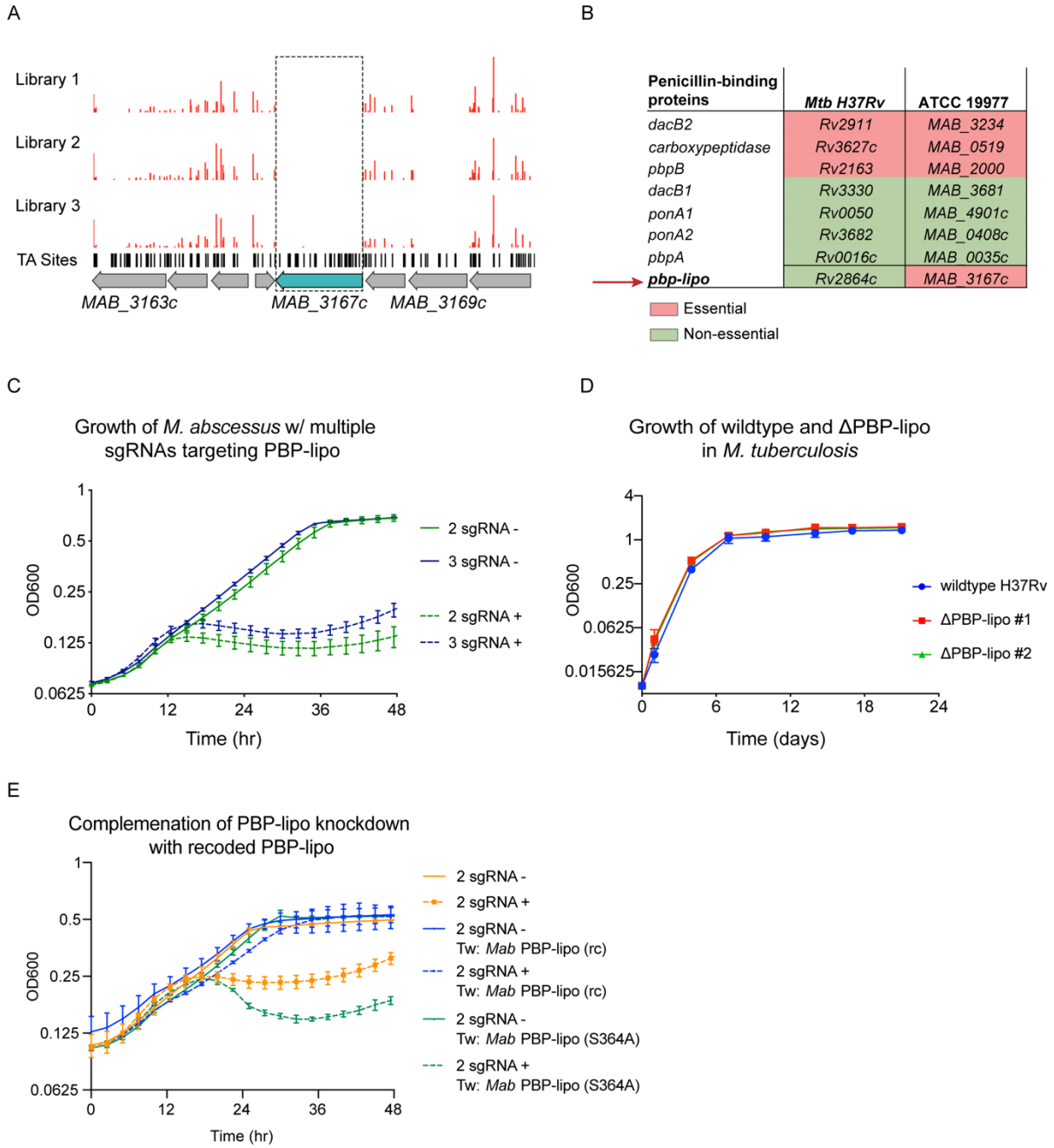

Figure 3. PBP-lipo is uniquely essential in *Mab* and non-essential in *Mtb*. (A) Transposon-insertion profile of PBP-lipo across three replicate transposon mutant libraries. Red bars indicate the number of transposon insertions. Horizontal black lines indicate 'TA' sites, where the transposon inserts. Genes are schematized with gray arrows, with PBP-lipo colored in blue. Dotted box demarcates lack of insertions in PBP-lipo. **(B)** Comparison of essentiality for PBP orthologs between *Mtb* and *Msm*. **(C)** Growth of *Mab* cultures transformed with CRISPRi plasmid carrying either 2 or 3 sgRNAs targeting PBP-lipo. "-" symbol indicates cultures were grown without ATc. "+" symbol indicates cultures were grown with ATc. **(D)** Growth of wildtype *Mtb* and PBP-lipo knockout strains. **(E)** Growth of *Mab* with native PBP-lipo knockdown complemented by recoded (rc) PBP-lipo, which sgRNAs can no longer bind. PBP-lipo (rc) (S364A) is a recoded and catalytically inactive version of the enzyme.

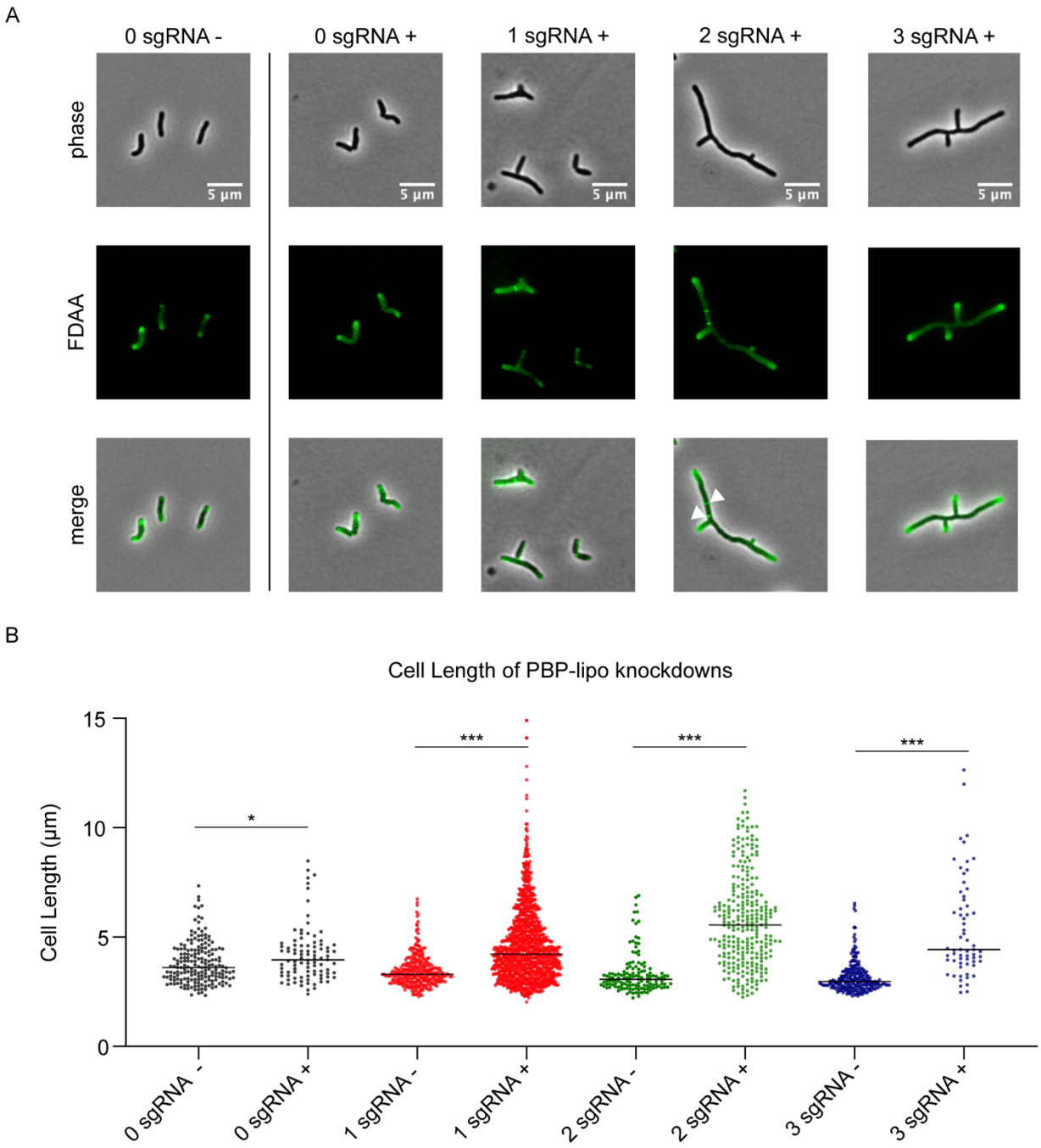

Figure 4. Knockdown of PBP-lipo disrupts cell morphology. **(A)** Microscopy images of PBP-lipo knockdown cultures. *Mab* strains carrying CRISPRi plasmids with either 0, 1, 2, or 3 sgRNAs targeting PBP-lipo. Arrows indicate sites of multiple septa formation. **(B)** Cell lengths of uninduced and induced strains. Measurements were obtained by GEMATRIA and MOMIA image analysis pipelines (35) . Student's *t test* used to calculate the statistical difference in mean cell lengths. *** = p-val < 0.0001. * = p-val < 0.05.

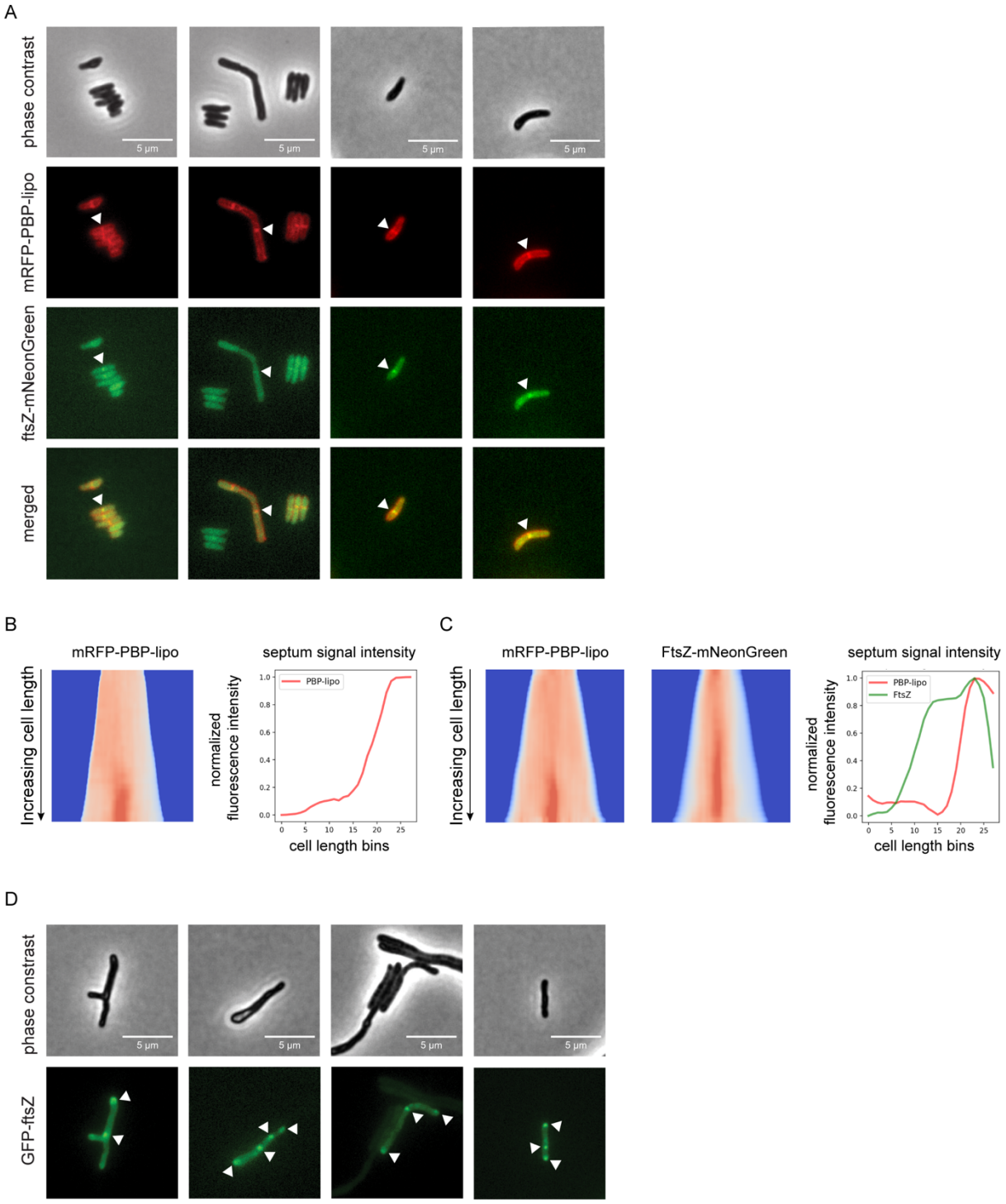

Figure 5. Knockdown of PBP-lipo disrupts formation of FtsZ rings. (A) Microscopy images of N-terminally tagged mRFP-PBP-lipo and C-terminally tagged FtsZ-mNeonGreen. 'Merged' images show overlay of red and green channels **(B)** (left) Demograph of mRFP-PBP-lipo. (right) Quantification of septal fluorescence signal across increasing cell lengths **(C)** (left) Demograph of mRFP-PBP-lipo and FtsZ-mNeonGreen. (right) Fluorescence signal arranged by increasing cell length **(D)** Images of GFP-FtsZ expressed from its natural promoter in the setting of PBP-lipo knockdown.

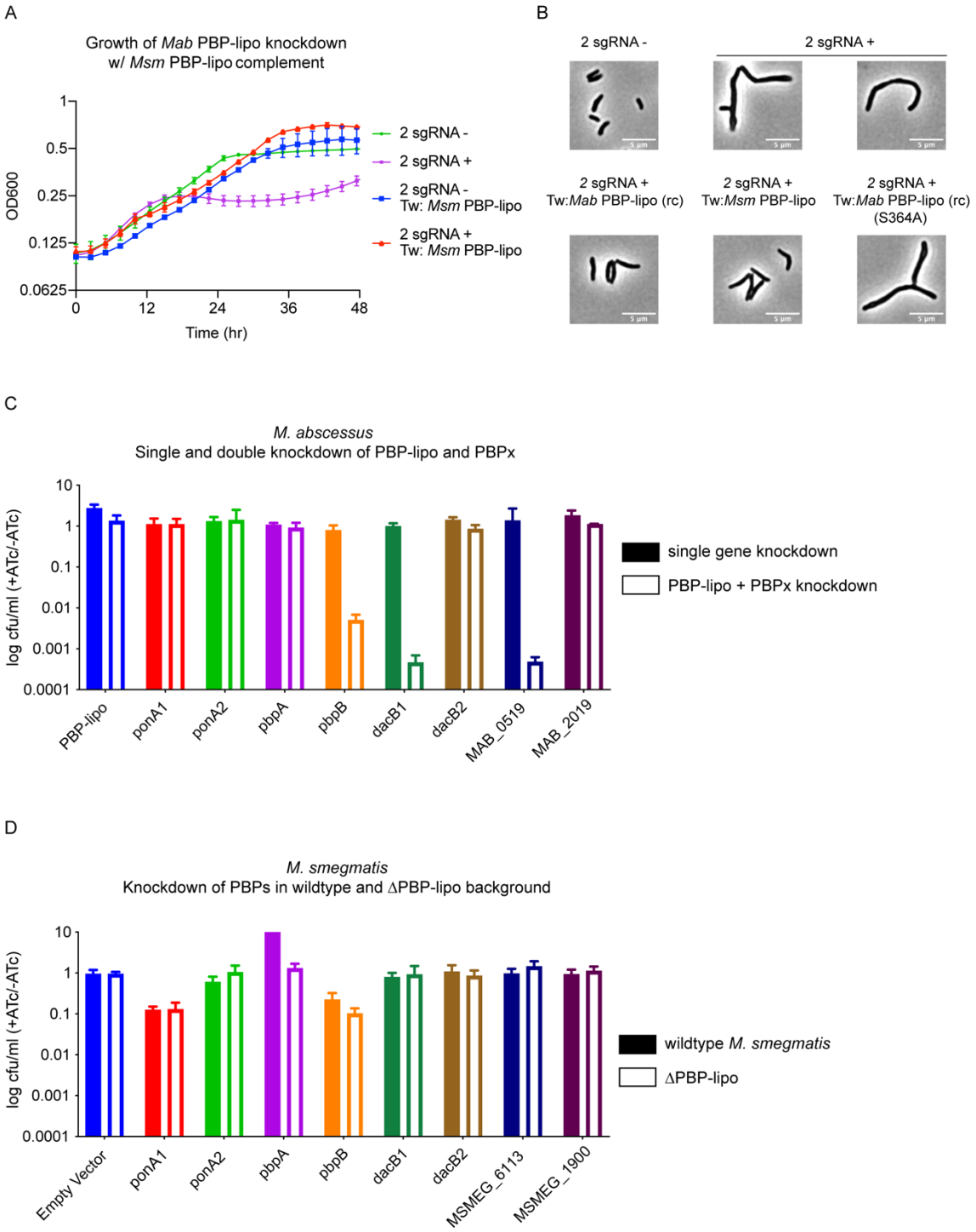

Figure 6. PBP-lipo network in *Mab* does not exist in *Msm*. (A) Growth curve of 2 sgRNA strain targeting PBP-lipo and 2 sgRNA strain constitutively expressing PBP-lipo$_{Msm}$. **(B)** Microscopy images of 2 sgRNA and PBP-lipo complement strains. **(C)** Genetic synergy of PBP-lipo with other PBPs in *Mab*. Solid bar represents CFU of strains where a single PBP was knocked down. Open bar represents strains where PBP-lipo was knocked down in combination with the listed PBP. **(D)** Genetic synergy of PBPs and PBP-lipo in *Msm.* CRISPRi plasmids carrying sgRNAs targeting each of the PBPs in *Msm* were transformed into wildtype *Msm* (closed bar) and the ΔPBP-lipo mutant (open bar).

1036
1037

Table 1: Minimum Inhibitory Concentration (MIC) (µg/ml) of ATCC 19977 +/- PBP-lipo Knockdown

Antibiotic	-ATc	+ATc	Fold Differencein MIC (-ATc/+ATc)
Cell Wall			
Ampicillin	>256	2	>128X
Amoxicillin	>256	2	>128X
Faropenem	8	1	8X
Cefoxitin	8	2	4X
Vancomycin	8	2	4X
Meropenem	128	128	N/A
Imipenem	>64	>64	“ “
Ticarcillin	>64	>64	“ “
Ceftazidime	>64	>64	“ “
Cephalexin	>64	>64	“ “
Ceftazidime	>64	>64	“ “
D-Cycloserine	>64	>64	“ “
Ethambutol	>64	>64	“ “
Isoniazid	>512	>512	“ “
Ribosome			
Clarithromycin	16	0.125	128X
Erythromycin	32	0.5	64X
Amikacin	16	4	4X
Clindamycin	>64	64	N/A
RNA Polymerase			
Rifampicin	32	2	16X
DNA Gyrase			
Ofloxacin	8	2	4X
Other			
Pyrazinamide	>64	>64	N/A
Pretomanid	>64	>64	“ “

1038
1039

1040

Table 2: MIC (µg/ml) of *Mab* Clinical Isolates +/- PBP-lipo knockdown (Cell Wall Antibiotics)

	Ampicillin			Amoxicillin			Meropenem	
Clinical Isolate	**-ATc**	**+ATc**		**-ATc**	**+ATc**		**-ATc**	**+ATc**
ATCC 19977	>256	2		>256	2		128	128
T35	>256	< 0.5		>256	< 0.5		>256	256
T37	>256	< 0.5		>256	< 0.5		>256	256
T49	>256	4		>256	4		>256	128
T50	>256	4		>256	4		>256	128
T51	>256	2		>256	2		>256	256
T53	>256	4		>256	2		>256	256
T56	>256	<0.5		>256	<0.5		>256	128
BWH-B	>256	8		>256	2		>256	256
BWH-C	>256	4		>256	8		>256	256
BWH-E	>256	4		>256	2		>256	256

1041
1042

1043

Table 3: MIC (µg/ml) of *Mab* Clinical Isolates +/- PBP-lipo Knockdown (Rifampicin and Clarithromycin)

	Rifampicin			Clarithromycin	
Clinical Isolate	**-ATc**	**+ATc**		**-ATc**	**+ATc**
ATCC 19977	32	2		16	0.125
T35	4	0.25		2	0.25
T37	16	1		2	0.25
T49	64	4		2	0.25
T50	32	1		16	0.25
T51	64	4		16	0.5
T53	32	1		8	0.5
T56	8	1		2	0.25
BWH-B	32	1		16	0.25
BWH-C	32	2		32	1
BWH-E	16	1		16	0.125

1044